INVESTIGATION OF THE STATIC UNIAXIAL STRAIN AND TRIAXIAL SHEAR RESPONSE OF CELLULAR CONCRETE

John Q. Ehrgott

Army Engineer Warerways Experiment Station
Vicksburg, Mississippi

May 1973

MISCELLANEOUS PAPER S-73-32

INVESTIGATION OF THE STATIC UNIAXIAL STRAIN AND TRIAXIAL SHEAR RESPONSE OF CELLULAR CONCRETE

by

J. Q. Ehrgott

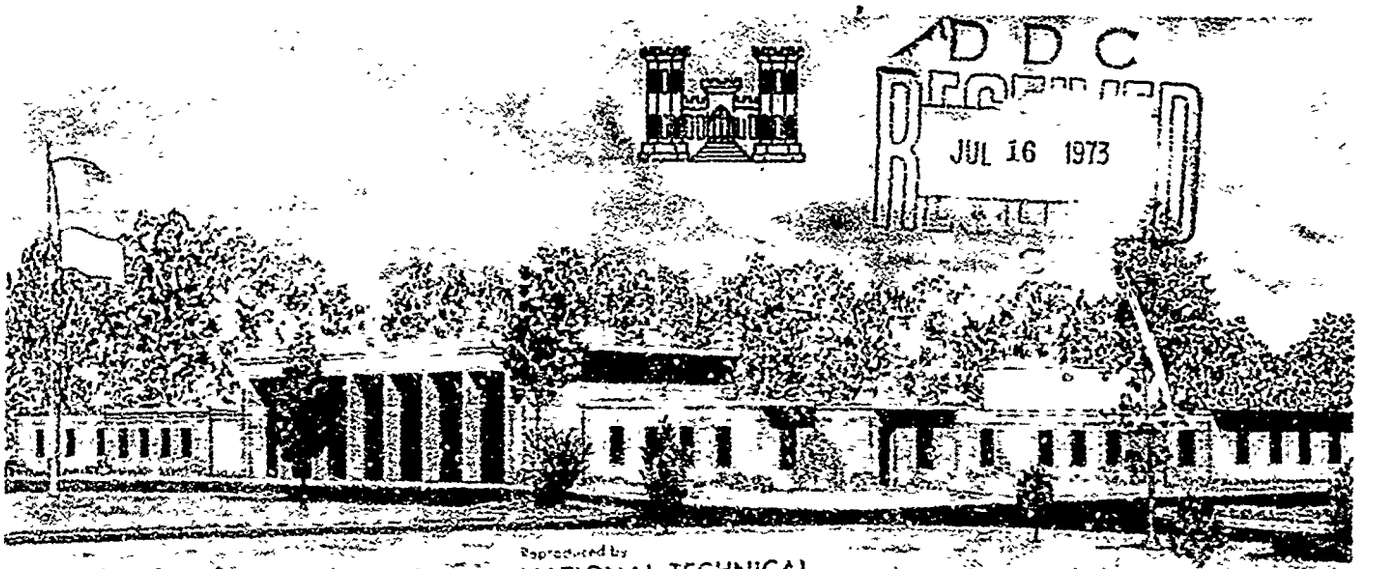

May 1973

Sponsored by U. S. Atomic Energy Commission and Defense Nuclear Agency
Subtask S&209, Work Unit 10, "Laboratory Evaluation of Gage Placement in Field Grout Mixtures"

Conducted by U. S. Army Engineer Waterways Experiment Station
Soils and Pavements Laboratory
Vicksburg, Mississippi

Unclassified
Security Classification

DOCUMENT CONTROL DATA - R & D

(Security classification of title, body of abstract and indexing annotation must be entered when the overall report is classified)

1. ORIGINATING ACTIVITY (Corporate author)
U. S. Army Engineer Waterways Experiment Station
Vicksburg, Mississippi

2a. REPORT SECURITY CLASSIFICATION
Unclassified

2b. GROUP

3. REPORT TITLE
INVESTIGATION OF THE STATIC UNIAXIAL STRAIN AND TRIAXIAL SHEAR RESPONSE OF CELLULAR CONCRETE

4. DESCRIPTIVE NOTES (Type of report and inclusive dates)
Final Report

5. AUTHOR(S) (First name, middle initial, last name)
John Q. Ehrgott

6. REPORT DATE	7a. TOTAL NO. OF PAGES	7b. NO. OF REFS
May 1973	63	2

8a. CONTRACT OR GRANT NO.	9a. ORIGINATOR'S REPORT NUMBER(S)
b. PROJECT NO.	Miscellaneous Paper S-73-32
c. Subtask SB209, Work Unit 10	9b. OTHER REPORT NO(S) (Any other numbers that may be assigned this report)
d.	

10. DISTRIBUTION STATEMENT
Approved for public release; distribution unlimited.

11. SUPPLEMENTARY NOTES	12. SPONSORING MILITARY ACTIVITY
	U. S. Atomic Energy Commission and Defense Nuclear Agency

13. ABSTRACT

Shock-absorbing concrete, cellular concrete, was developed and used in several experiments at the Nevada Test Site to reduce or attenuate ground shock produced from blast loadings. In conjunction with the field experiments, an analytical investigation involving the use of computer calculations to predict the shock propagation through the concrete was also initiated. One of the requirements of this effort involving computer codes was the development of constitutive relations of the concrete. This report documents the results of laboratory tests conducted on a 62-pcf-density cellular concrete to determine the static response of the concrete. An effort was made to test the mix in several states of stress, including uniaxial strain, hydrostatic compression, and triaxial shear, to determine the response aspects considered most important in the development of its constitutive properties. Representative static stress-strain curves of 62-pcf-density cellular concrete are presented ranging to stress levels as high as 8,000 psi for each of the several stress states investigated.

DD FORM 1 NOV 68 1473 REPLACES DD FORM 1473, 1 JAN 64, WHICH IS OBSOLETE FOR ARMY USE.

Unclassified
Security Classification

14 KEY WORDS	LINK A		LINK B		LINK C	
	ROLE	WT	ROLE	WT	ROLE	WT
Cellular concretes						
Constitutive relations						
Ground shock						
Shock absorption						

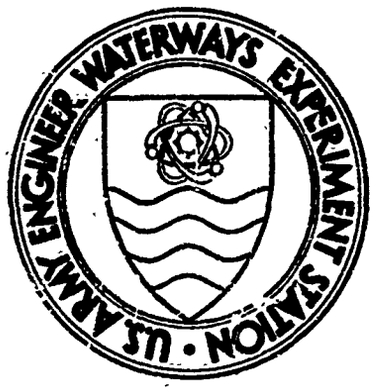

MISCELLANEOUS PAPER S-73-32

INVESTIGATION OF THE STATIC UNIAXIAL STRAIN AND TRIAXIAL SHEAR RESPONSE OF CELLULAR CONCRETE

by

J. Q. Ehrgott

May 1973

Sponsored by U. S. Atomic Energy Commission and Defense Nuclear Agency
Subtask SB209, Work Unit 10, "Laboratory Evaluation of Gage Placement in Field Grout Mixtures"

Conducted by U. S. Army Engineer Waterways Experiment Station
Soils and Pavements Laboratory
Vicksburg, Mississippi

ABSTRACT

Shock-absorbing concrete, cellular concrete, was developed and used in several experiments at the Nevada Test Site to reduce or attenuate ground shock produced from blast loadings. In conjunction with the field experiments, an analytical investigation involving the use of computer calculations to predict the shock propagation through the concrete was also initiated. One of the requirements of this effort involving computer codes was the development of constitutive relations of the concrete.

This report documents the results of laboratory tests conducted on a 62-pcf-density cellular concrete to determine the static response of the concrete. An effort was made to test the mix in several states of stress, including uniaxial strain, hydrostatic compression, and triaxial shear, to determine the response aspects considered most important in the development of its constitutive properties. Representative static stress-strain curves of 62-pcf-density cellular concrete are presented ranging to stress levels as high as 8,000 psi for each of the several stress states investigated.

PREFACE

This report documents the results of an experimental program conducted on a shock-absorbing concrete, cellular concrete, for the Sandia Laboratories, Albuquerque, New Mexico, during the period of April through June 1971, by personnel of the Soils and Pavements Laboratory, U. S. Army Engineer Waterways Experiment Station (WES), Vicksburg, Mississippi. The testing program was funded by the U. S. Atomic Energy Commission; report preparation was funded by the Defense Nuclear Agency; and the effort was coordinated by Mr. C. W. Gulich, Jr., of Sandia Laboratories.

Mr. G. C. Hoff, Engineering Mechanics Branch, Concrete Laboratory, WES, provided the specimens and information on the cellular concrete, which the Concrete Laboratory had developed for the Sandia Laboratories for use in several experiments at the Nevada Test Site.

The laboratory tests were conducted by Mr. E. E. Chisolm, and the results were analyzed by Mr. J. Q. Ehrgott, under the supervision of Mr. P. F. Hadala and Dr. J. G. Jackson, Jr., all of the Soil Dynamics Division. This report was prepared by Mr. Ehrgott. During the conduct of the study, Mr. J. P. Sale was Chief of the Soils and Pavements Laboratory.

COL Ernest D. Peixotto, CE, was Director of the WES during the preparation and publication of this report. Mr. F. R. Brown was Technical Director.

CONTENTS

NOTATION

G	Shear modulus
G_i	Initial loading shear modulus
K	Bulk modulus
K_o	Earth pressure at rest
M	Constrained modulus
p	Mean normal stress
Δp	Mean normal stress change
V_o	Original volume of test specimen
ΔV	Volume change
$\Delta V/V_o$	Volumetric strain
w	Water content
γ	Wet unit weight
γ_d	Dry unit weight
ϵ_a	Axial strain
ϵ_r	Radial strain
$\epsilon_a - \epsilon_r$	Principal strain difference
σ_a	Axial stress
$\Delta\sigma_a$	Axial stress change
σ_r	Radial stress
$\Delta\sigma_r$	Radial stress change
$\sigma_a - \sigma_r$	Principal stress difference
$(\sigma_a - \sigma_r)_{max}$	Peak principal stress difference
$\Delta(\sigma_a - \sigma_r)$	Principal stress difference change

CONVERSION FACTORS, BRITISH TO METRIC UNITS OF MEASUREMENT

British units of measurement used in this report can be converted to metric units as follows:

Multiply	By	To Obtain
inches	2.54	centimeters
feet	0.3048	meters
pounds (force) per square inch	0.6894757	newtons per square centimeter
kips (force) per square inch	0.6894757	kilonewtons per square centimeter
pounds per cubic foot	16.01846	kilograms per cubic meter

CHAPTER 1

INTRODUCTION

The U. S. Army Engineer Waterways Experiment Station (WES), under Defense Nuclear Agency sponsorship, has developed a shock-absorbing, backpacking material (cellular concrete) for use around deeply buried structures. An extensive program has been conducted to design the material with certain required shock-absorbing properties, to develop field placement techniques for the designed material, and to develop field tests to monitor the properties of the in-place material.

The material developed from that project has been used during several field events at the Nevada Test Site in conjunction with a program carried out by the Sandia Laboratories. The field and laboratory tests performed to date on cellular concrete have provided insight into its behavioral characteristics and the design parameters that control its response. However, there is currently a need by Sandia Laboratories to determine the constitutive properties of cellular concrete to be used as input for analytical studies of the propagation of ground shock through cellular concrete. WES was requested by Sandia Laboratories to define the constitutive properties of cellular concrete. The funding for this work was provided by the U. S. Atomic Energy Commission.

1.1 PURPOSE

The purpose of this study was to conduct experimental laboratory tests on specimens of cellular concrete to determine the constitutive properties of the material that would be needed for the derivation of constitutive relations in terms of stress invariants.

1.2 SCOPE

This report documents the results of a series of 20 tests to define the static behavior of cellular concrete under a variety of controlled states of stress and it describes the analyses of the test data to determine representative stress-strain relations that are thought to be most important for use in the development of constitutive relations

for use in computer code solutions of two-dimensional continuum mechanics boundary value problems.

CHAPTER 2

DESCRIPTION OF EXPERIMENTAL PROGRAM

The tests conducted under this study included uniaxial (UX) strain tests, special UX tests with measurement of radial stress (null tests), and triaxial (TX) tests with a hydrostatic loading portion and a shear portion. The UX and null tests required wafer-shaped specimens, generally 5 inches[1] in diameter by 2-1/2 inches high. However, it was also possible to conduct tests on 5-inch-diameter by 1-inch-high specimens in the UX test device. Cylindrically shaped specimens were required for the TX tests; the specimens used in this part of the study were 2-1/8 inches in diameter by 5 inches long.

2.1 SPECIMEN PREPARATION

In general, cellular concrete is the name given to a family of low-density, air-entrained concretes. Many of the physical properties of this class of materials are documented in Reference 1. All of the tests conducted in this study were performed on specimens cast from the same batch of concrete, which had a design density of 62 pcf. All of the specimens were cured at room temperature. Part of the material was poured into pasteboard tubes that were 3 inches in diameter by 3 feet long. TX test specimens were later obtained from the tube-encased material. A second portion was poured into steel rings, 5 inches in diameter by 2-1/2 inches high. Immediately after pouring, the tube specimens and the 2-1/2-inch-high steel ring specimens were sealed in plastic bags to prevent air exposure. The remaining material, which was poured into 1-inch-high by 5-inch-diameter steel rings, was covered only with a light cardboard cover, which did not prevent exposure to air.

The material in the steel rings was used for the UX tests. The exposed ends were trimmed down level with the top and bottom edges of the

---

[1] A table of factors for converting British units of measurement to metric units is presented on page 8.

steel ring. The waste pieces of material obtained from the trimmings were used for water content determinations. The material in the rings was weighed for density determinations prior to its placement in the test device.

The material in the pasteboard tubes was used for the TX tests. A 5-1/2-inch-long section was cut from each 3-foot-long tube. The piece was placed in a standard laboratory device for trimming soil specimens, and a knife was used to cut the 3-inch diameter down to 2-1/8 inches. The specimen was then placed in a 5-inch-long miter box, and the ends were cut perpendicular to the specimen axis. The waste material obtained from the trimmings was used for water content determinations. The dimensions and weight of each specimen were measured prior to placement in the test device.

2.2 CONDUCT OF UNIAXIAL STRAIN TESTS

The WES UX test device used in this study is described in Reference 2. The device operates in conjunction with a separate pneumatic ram loader to produce axial stress levels as high as 2,000 psi on specimens 5 inches in diameter by either 1 inch or 2-1/2 inches high. The ram loader compresses a fluid in the device, which produces a uniform pressure across the top of the specimen. A rigid steel boundary around the specimen prevents lateral expansion of the specimen; i.e., there is no lateral strain. Measurements of the applied pressure and axial deflection of the specimen's surface are made continuously during the test. The pressure and deflection data can then be used to calculate the axial stress σ_a and axial strain ϵ_a, which are plotted to produce a curve whose slope is the constrained modulus M.

2.3 CONDUCT OF NULL TESTS

The WES null test device is similar to the UX device; however, the rigid steel boundary is replaced by a second fluid container that can be pressurized by compressed gas. The specimen, 5 inches in diameter by 2-1/2 inches high, must be contained in a thin, 1/8-inch-thick steel ring. The outside of the steel ring is strain-gaged prior to placement

in the device. As the specimen is loaded in the axial direction, the output of the strain gages is monitored. The second fluid container is pressurized as required to keep the output of the strain gages at zero. Measurements of the axial pressure, axial deflection, and pressure required to prevent lateral ring movement are made. The data are then used to calculate axial stress σ_a, axial strain ϵ_a, and radial stress σ_r. The axial stress and strain can be plotted to produce a curve whose slope is M. The axial and radial stresses can be plotted to produce a curve whose slope is K_o, earth-pressure-at-rest, which for elastic material is related to Poisson's ratio ν as

$$\nu = \frac{K_o}{1 + K_o} \tag{2.1}$$

2.4 CONDUCT OF TRIAXIAL TESTS

The TX tests were conducted in two test phases. First, each specimen was enclosed in a rubber membrane and placed in the test device, and a hydrostatic test was conducted by loading the specimen with equal fluid pressure from all directions. Measurements of the pressure, the change in the specimen's height, and the change in the specimen's center diameter were made during the hydrostatic portion of the test. These measurements were used to calculate mean normal stress p and volumetric strain $\Delta V/V_c$, which can be plotted to produce a curve whose slope is the bulk modulus K. The shear phase of the test was conducted after the hydrostatic phase. The peak pressure reached during the hydrostatic test was held constant, and a piston was used to apply additional load to the specimen in the axial direction. The load was increased until the specimen could not support additional load. Measurements of the confining pressure, axial load, and specimen height and diameter changes made during the additional axial loading were used to calculate radial stress σ_r, principal stress difference $\sigma_a - \sigma_r$, axial strain ϵ_a, radial strain ϵ_r, and principal strain difference $\epsilon_a - \epsilon_r$. A plot of principal stress difference versus principal strain difference produces a curve whose slope is two times the shear modulus G. The peak

deviator stresses from several tests conducted at different levels of confining pressure can be plotted as peak principal stress difference $(\sigma_a - \sigma_r)_{max}$ versus mean normal stress $p = (\sigma_a + 2\sigma_r)/3$. These points describe the failure envelope of the material.

2.5 SPECIMEN COMPOSITION PROPERTIES

Measurements of water content w , wet unit weight γ , and dry unit weight γ_d for each of the specimens tested are presented in Table 2.1. As described in this report, water content is the ratio of the weight of water to the weight of dry material; wet unit weight is the weight of the material per unit volume; and dry unit weight is the weight of a dry material per unit volume. Also presented in Table 2.1 is the cure time for each specimen. Cure time is the time from the molding of the concrete batch until the material is trimmed and tested.

The specimens used in the TX tests had cure times of from 35 to 61 days. The average water content and wet and dry unit weights were approximately 49 percent, 61 pcf, and 41 pcf, respectively. The average properties of the 2-1/2-inch UX and null test specimens were approximately the same as those of the TX specimens. The UX specimens in the 1-inch-high steel rings were drier than the specimens in the 2-1/2-inch-high rings. The 1-inch specimens had average w , γ , and γ_d of 26 percent, 53 pcf, and 42 pcf, respectively. The reason for the difference can probably be traced back to the storage of the specimens. The TX, the null, and the 2-1/2-inch UX specimens were sealed in plastic bags, but the 1-inch UX specimens were not sealed and undoubtedly lost moisture while exposed to the air.

TABLE 2.1 COMPOSITION PROPERTY DATA FOR CELLULAR CONCRETE SPECIMENS

UX, unaxial strain test; N, null test; TX, triaxial test; S, static; D, dynamic; NA, not available.

Test No.	Cure Time	Type Test	Water Content w	Wet Unit Weight γ	Dry Unit Weight γ_d	TX Confining Pressure σ_r	Remarks
	days		pct	pcf	pcf	ksi	
U-1	21	UX-S	NA	NA	NA	--	--
U-2	21	UX-D	NA	NA	NA	--	--
U-3	24	UX-D	NA	NA	NA	--	--
U-4	35	UX-S	27.4	53.6	42.1	--	--
U-5	38	UX-D	26.6	53.4	42.2	--	--
U-7	41	UX-S	25.4	53.2	42.4	--	--
U-8	41	UX-S	47.1	61.2	41.5	--	--
N-6	38	N-S	48.0	62.9	42.5	--	--
N-9	54	N-S	43.3	61.1	42.6	--	--
T-1	33	TX-S	45.1	--	--	--	Leak during test
T-2	35	TX-S	49.6	61.2	40.9	0.517	--
T-3	35	TX-S	49.5	61.7	41.3	2.020	--
T-4	35	TX-S	49.4	67.1	44.9	5.100	Hard spot in specimen
T-5	59	TX-S	48.7	61.9	41.6	1.300	No axial measurement during hydrostatic loading
T-6	60	TX-S	48.9	60.5	40.6	1.500	Voids noted in specimen
T-7	60	TX-S	50.0	61.7	41.1	3.300	--
T-8	60	TX-S	50.1	61.1	40.7	7.600	--
T-9	61	TX-S	45.9	58.9	40.4	0.000	Voids noted in specimen
T-10	61	TX-S	47.7	62.1	42.0	1.000	--
T-11	61	TX-S	NA	62.0	NA	4.000	--

CHAPTER 3

CONSTITUTIVE PROPERTY TESTS

3.1 UNIAXIAL TEST RESULTS

A series of four static UX and two null tests were conducted for this study. The axial stress versus axial strain curves from the static UX and null tests are presented in Figure 3.1. Also shown in Figure 3.1 is a list of the specimen height, cure time, water content, and wet and dry unit weights for each of the tests. It should be noted that three of the tests, U-1, U-4, and U-7, were conducted on 1-inch specimens that were allowed to dry during storage.

The general trend of the test results shown in Figure 3.1 indicates that the material has a relatively stiff initial constrained modulus M , followed by a softening or increased rate of strain with increasing stress at approximately 800-psi axial stress. The material continues to strain to approximately 25 percent axial strain, after which the rate of strain rapidly decreases and the stress-strain curve begins to stiffen. Since the specimens were unloaded at stress levels below 2,000 psi, their behavior at higher pressures was not determined. However, it is assumed, based on the available data, that the material would continue to stiffen and approach a locked condition at saturation at approximately 40 to 45 percent axial strain.

The initial portion of the uniaxial strain response of the material is probably controlled by the strength of the particle bonds of the material. The sudden increase in rate of straining may be related to the structural breakdown, or collapse, of these bonds. As the material is loaded, complete collapse of the major bonds occurs, and the amount of strain the material undergoes may be related to the empty void space available to be filled by the broken particles. As what was formerly air-filled void space becomes filled with the solids and free water, the material stiffens and approaches a locked condition. The only tests loaded to stress levels high enough to show such behavior were those of the dried material, Tests U-1 and U-4. However, it is reasonable to

assume that the wetter material would have begun to stiffen at lesser strain levels, since the wetter material contained a smaller air-void content and more free water.

Figure 3.2 is an enlarged view of the initial stress-strain plot for five of the tests, U-4, U-7, N-6, N-9, and U-8. Since the purpose of Test U-4 was to define the response of the material to 40 percent strain, the accuracy of this test shown on the strain scale used in Figure 3.2 is questionable. Tests U-7, N-6, N-9, and U-8 were conducted only to relatively small strain levels, and the results were used to determine the initial M. Test N-6 was cycled at axial stress levels of 100, 300, and 500 psi, and the results indicate a hysteretic behavior of the material even in the initial loading portion prior to what is believed to be the onset of structural collapse.

The dynamic UX tests conducted in this study were intended to provide some means by which the static data could be qualitatively adjusted to reflect dynamic conditions. The dynamic test results are shown in Figure 3.3. The tests were conducted on 1-inch specimens; therefore, the results can only be compared with static Tests U-1, U-4, and U-7 shown in Figure 3.1.

3.2 NULL TEST RESULTS

Two static null tests, N-6 and N-9, were conducted on 2-1/2-inch-high specimens. The axial stress/axial strain curves for these tests are presented in Figures 3.1 and 3.2.

The null test data may also be used to calculate deviator stress $\sigma_a - \sigma_r$ and mean normal stress $p = (\sigma_a + 2\sigma_r)/3$ and may be plotted as a stress path $\sigma_a - \sigma_r$ versus p. Because the material is tested in a condition of uniaxial strain, i.e., $\epsilon_r = 0$, the slope of the stress path curves can be related to Poisson's ratio ν for an incremental elastic material as curve slope

$$S = \frac{\Delta(\sigma_a - \sigma_r)}{\Delta p} \tag{3.1}$$

and, since earth-pressure-at-rest

$$K_o = \frac{\Delta\sigma_r}{\Delta\sigma_a} = \frac{\nu}{1 - \nu} \tag{3.2}$$

then,

$$K_o = \frac{3 - S}{2S + 3} \tag{3.3}$$

By substitution,

$$\nu = \frac{3 - S}{S + 6} \tag{3.4}$$

The stress paths for Tests N-6 and N-9 are shown in Figure 3.4. The slope of the curve indicates an initial low value of Poisson's ratio, which increases as the stress level increases. Unloading appears to give lower values to Poisson's ratio than are indicated during loading. The results of Test N-9 were suspect beyond a mean normal stress of 570 psi because of the following development. Test N-9 was loaded to 1,000-psi axial stress without noticeable structural collapse. At 1,000 psi, application of the axial stress was stopped. While the fluid pressure used to load the specimen was held constant, the material suddenly began to strain. The sudden decrease in specimen volume resulted in a decrease in fluid pressure before the test operator could adjust the pressure level. The axial pressure was then increased to approximately 1,250 psi prior to unloading, but adjustment of the radial pressure to maintain no lateral strain in unloading was difficult.

3.3 TRIAXIAL TEST RESULTS

3.3.1 Hydrostatic Phase. A series of nine hydrostatic tests were conducted at peak hydrostatic pressures as high as 7,600 psi. Upon reaching the desired peak pressure for each test, the pressure (i.e., the confining pressure) was held constant while a shear test was conducted. However, in three of the tests, the specimens were subjected to cycled hydrostatic loading prior to reaching peak pressure in order to obtain unloading-reloading hydrostatic response data. The mean normal stress versus volumetric strain curves for the hydrostatic

phase of the tests are presented in Figures 3.5 and 3.6. The test results are shown to a stress of 7,000 psi in Figure 3.5 and are replotted to an expanded stress scale in Figure 3.6. Also listed in Figure 3.5 are the cure time, water content, and wet and dry unit weights of each of the specimens.

In general, the hydrostatic pressure/volumetric strain curves or hydrostats are similar to the UX test axial stress/axial strain curves for this material. The material has an initial stiff bulk modulus to approximately 600-psi mean normal stress, followed by a marked increase in strain with increasing stress. The material appears to increase in stiffness at approximately 1,500 psi and reaches a maximum stiffness or maximum K (for the stress levels studied) at approximately 4,000- to 5,000-psi mean normal stress. The apparent resoftening of the specimen in Test T-8 at 5,500 psi, shown in Figure 3.5, could be erroneous data or could be a phenomenon associated with secondary collapse of material. The test results do, however, appear reasonable and consistent considering the variations in material cure time and properties.

The unloading-reloading portions of Tests T-3 and T-4, as shown in Figure 3.6, indicate a relatively stiff response of the material. The large hook or strain recovery noted at low levels of stress in Test T-4 appears questionable. It is not known if the material did, in fact, recover the amount indicated or if the axial measurement system was in error due to a lifting of the specimen top cap. The reloading portions of the two tests appear reasonable.

It should also be noted that the specimen in Test T-4 contained a hard spot or a nodule of greater density. This resulted in an overall increase in density for Test T-4 and also may have resulted in a slightly stiffer loading hydrostat.

Figure 3.7 is an enlarged scale plot of the initial loading portion of several of the tests shown in Figures 3.5 and 3.6. During the first 20 psi, the results are questionable, which could be due to the top cap seating on the specimen. Test T-2 was cycled at 200 and 350 psi, and the results indicate a hysteretic response behavior of the material even under relatively low stress levels.

3.3.2 Shear Phase. The results of the shear portions of the TX tests are shown in Figures 3.8 through 3.11 as plots of principal stress difference versus the axial and radial strains. The levels of constant confining pressure σ_r at which the tests were conducted are listed in each figure.

The sign convention used throughout this report is for compression as positive; therefore, in the shear test plots, a negative radial strain represents specimen lateral expansion. It should also be noted in connection with Figures 3.8 through 3.11 that the strains were re-zeroed at the start of the shear test portion.

The test data were also used to construct a plot of principal stress difference versus principal strain difference for each test. Figure 3.12 shows this type of plot for each of the shear tests. The slope of each of the curves is $2G$. The results indicate an increase in the initial value of G with increasing confining pressure, beginning with Test T-2 conducted at 517 psi. One test, T-9, was conducted at a lower pressure, 0 psi. The initial slope of Test T-9 is higher than those for tests conducted at confining pressures below 2,000 psi; however, based on the trend of the other test results, it is doubtful that the results of Test T-9 are valid.

Figure 3.12 also shows a general increase in rate of strain with increasing deviator stress. The rate of straining appears to be greatest at the lower confining pressures and decreases with increasing confining pressure to 1,500 psi. Above 3,000-psi confining pressure, the stress-strain curves show little softening effect, and peak deviator stress is reached at relatively low values of deviator strain.

Only one test, T-6, was cycled during the shear test phase. The results indicate a stiff unloading-reloading shear modulus. Without additional testing, the unloading-reloading response at other levels of confining pressure and deviator stress can only be assumed to show the same general trend.

Figure 3.13 is a plot of principal stress difference versus mean normal stress showing the states of stress at failure for the TX tests. The failure stress for each test was selected as being either the peak

principal stress difference or the level of principal stress difference associated with 15 percent principal strain difference, whichever occurred first. The corresponding mean normal stress at failure was calculated from

$$p = \left(\frac{\sigma_a - \sigma_r}{3}\right)_{max} + \sigma_r \qquad (3.5)$$

It should be noted that the stress path the material followed up to failure in a constant confining pressure shear test plots as a 3:1 slope in Figure 3.13 (see the dashed lines). Unlike the uniaxial strain test results, the path of a shear test, when plotted on the stress path, is not a function of the material properties.

The failure data plotted in Figure 3.13 appear consistent except for Test T-9. The failure deviator stress is somewhat higher than the trend suggested by the rest of the data. In general, at low levels of p (<500 psi), the envelope may be flat and similar to the envelope of a cohesive or bonded material. At midrange levels of p (500 to 2,400 psi), the envelope appears similar to that of a cohesionless material. Beyond 2,400 psi, the envelope begins to flatten again. This development is probably due to the fact that the material is approaching saturation. The envelope becomes quite flat at a $p > 5{,}000$ psi. The fact that the failure stress of Test T-8 is somewhat higher than that of Tests T-11 and T-4 could be due to data scatter or related to the secondary compaction noted previously in the hydrostatic data. The strength envelope for this material is believed to be best represented by a flat line above 9 ksi mean normal stress.

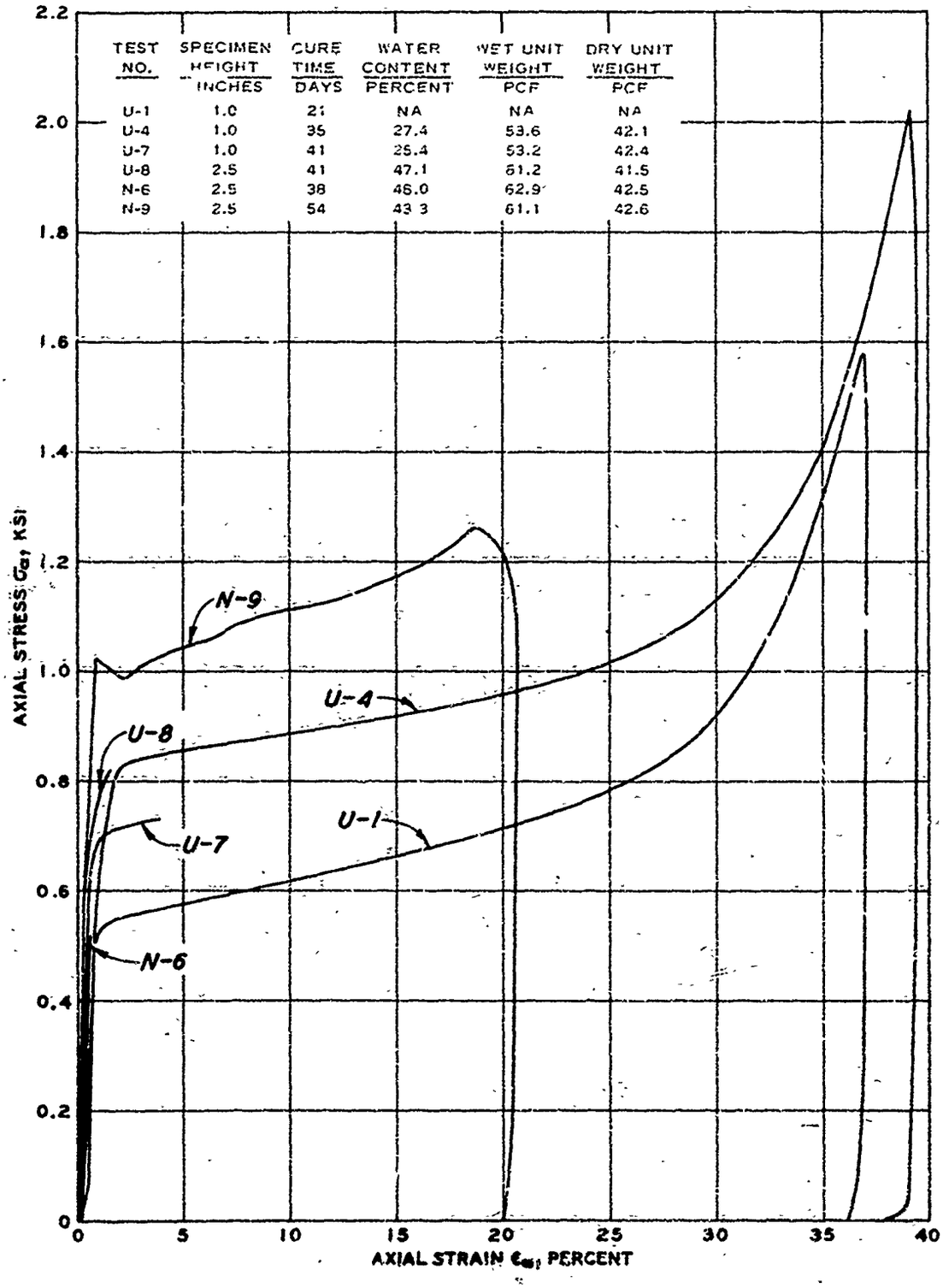

Figure 3.1 Static uniaxial and null test results.

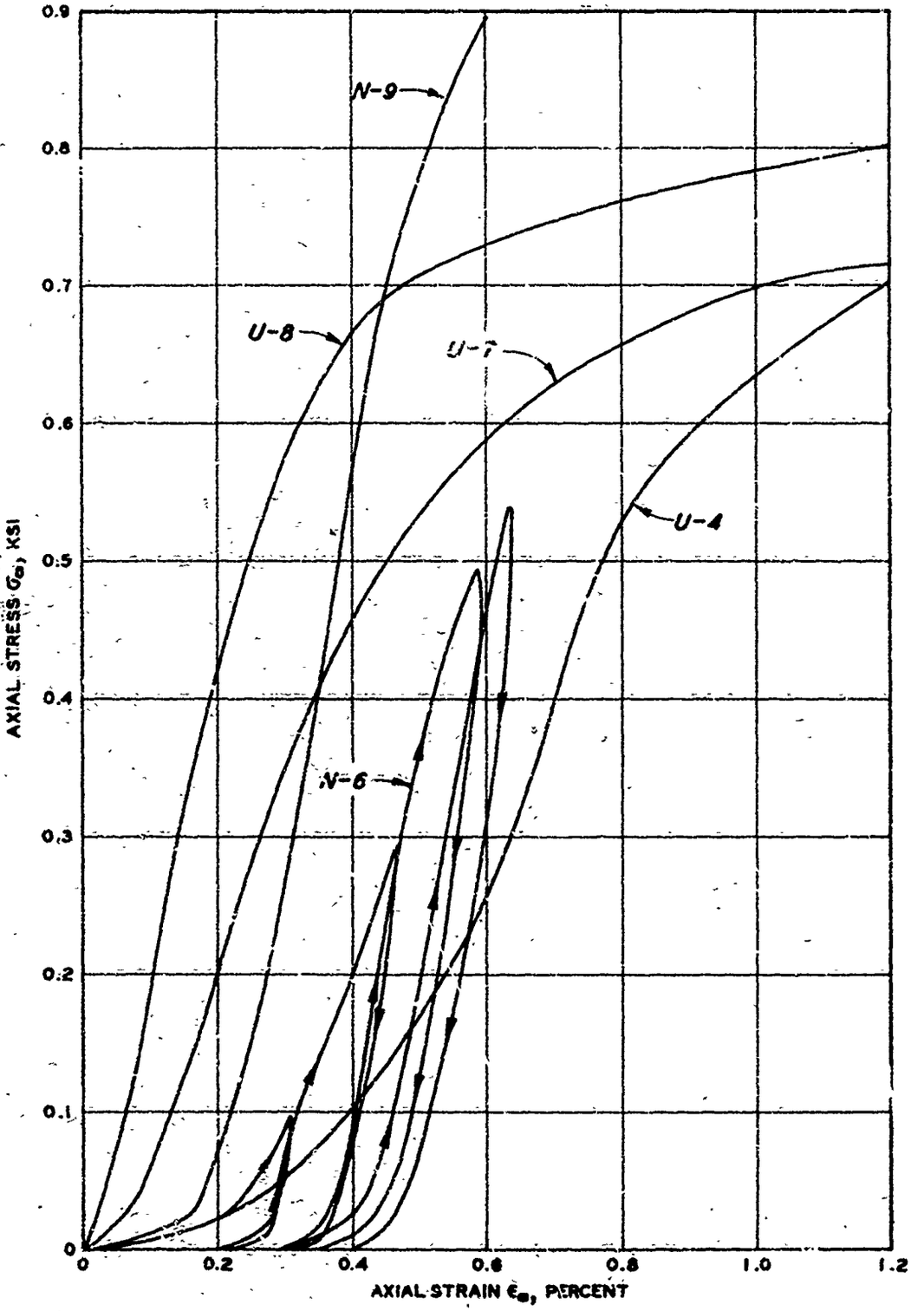

Figure 3.2 Static uniaxial and null test results showing initial loading response.

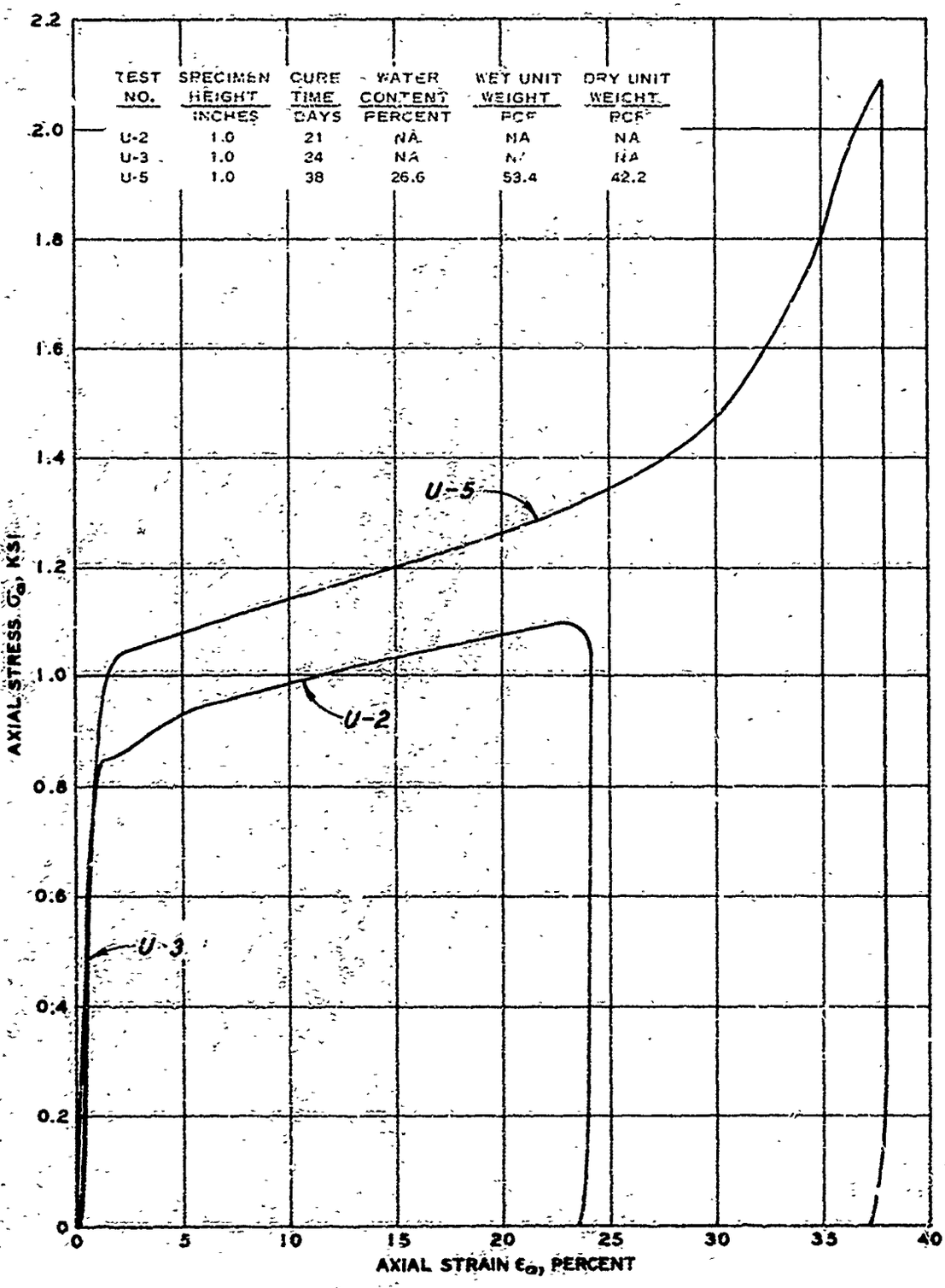

Figure 3.3 Dynamic uniaxial test results.

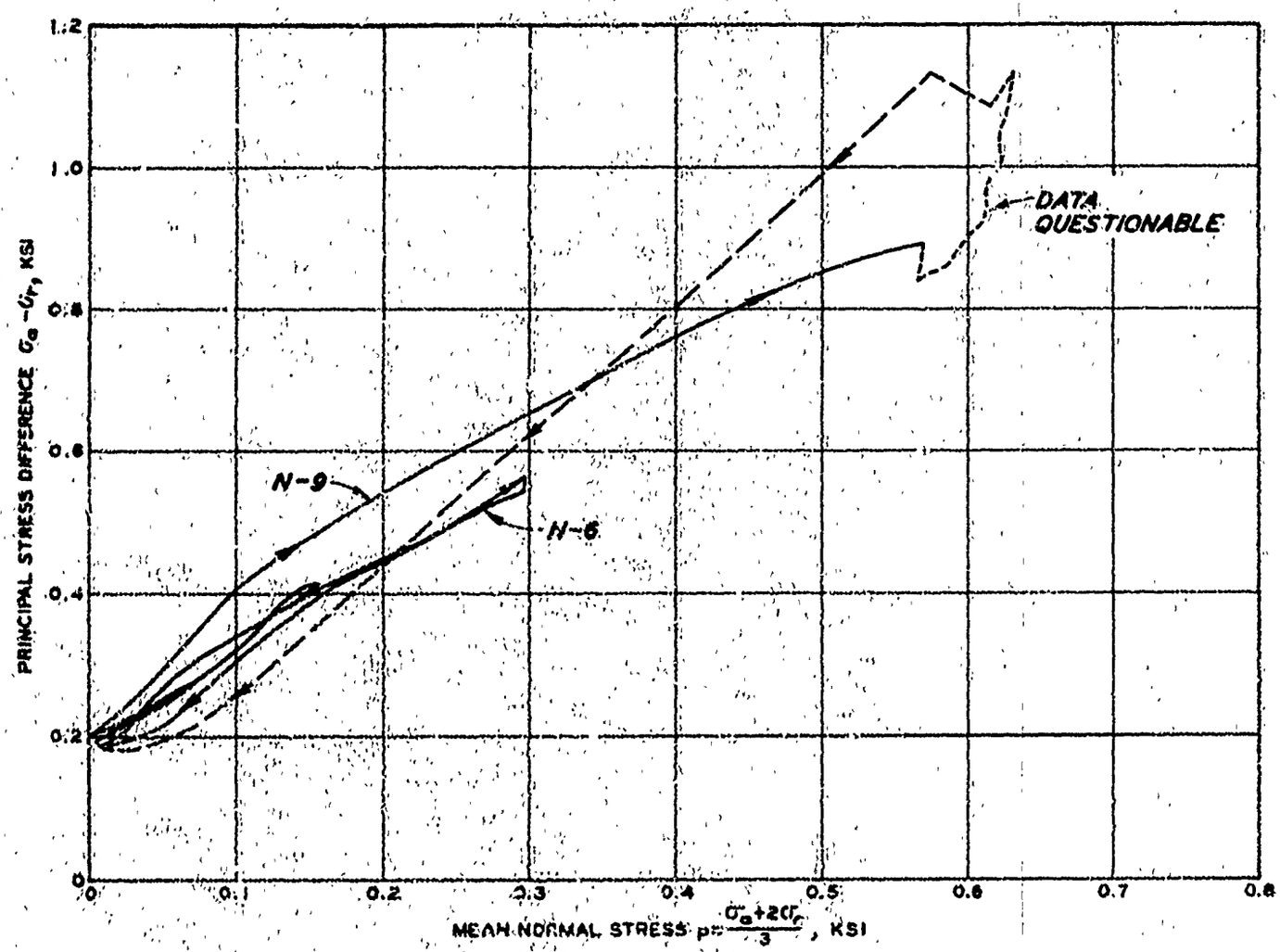

Figure 3.4 Results of two null tests showing uniaxial stress path.

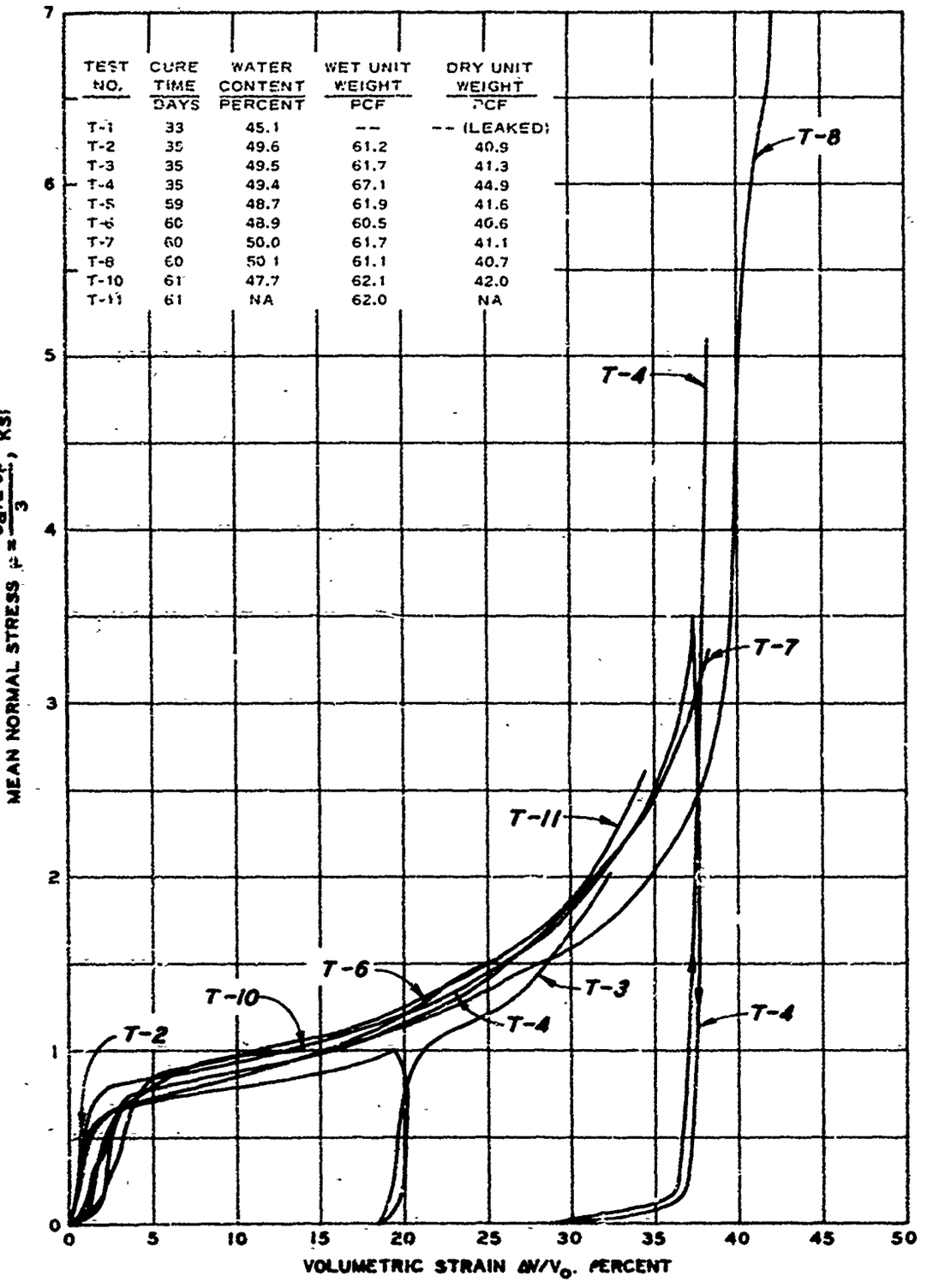

Figure 3.5 Static hydrostatic test results.

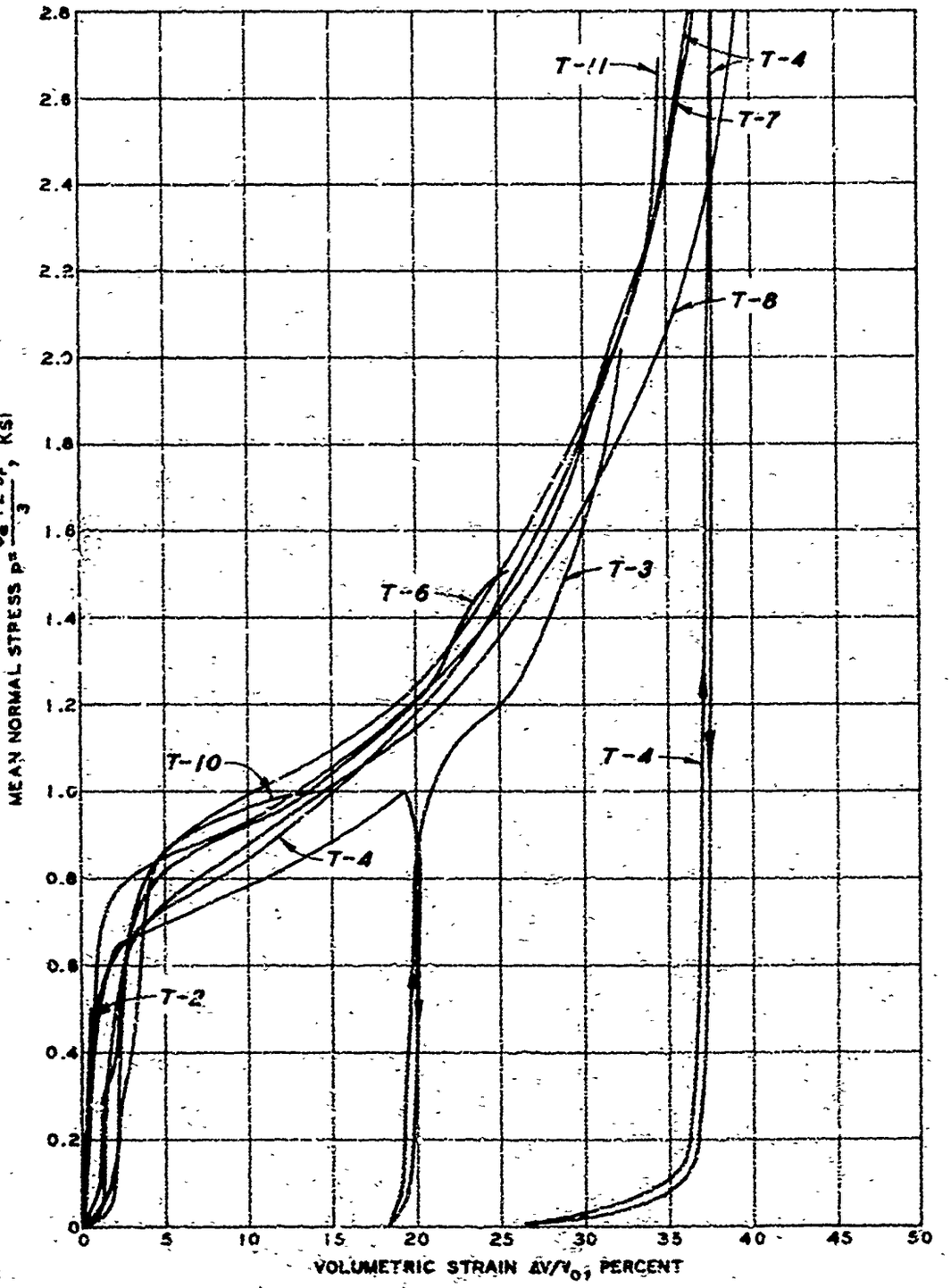

Figure 3.6 Enlarged plot of static hydrostatic test results.

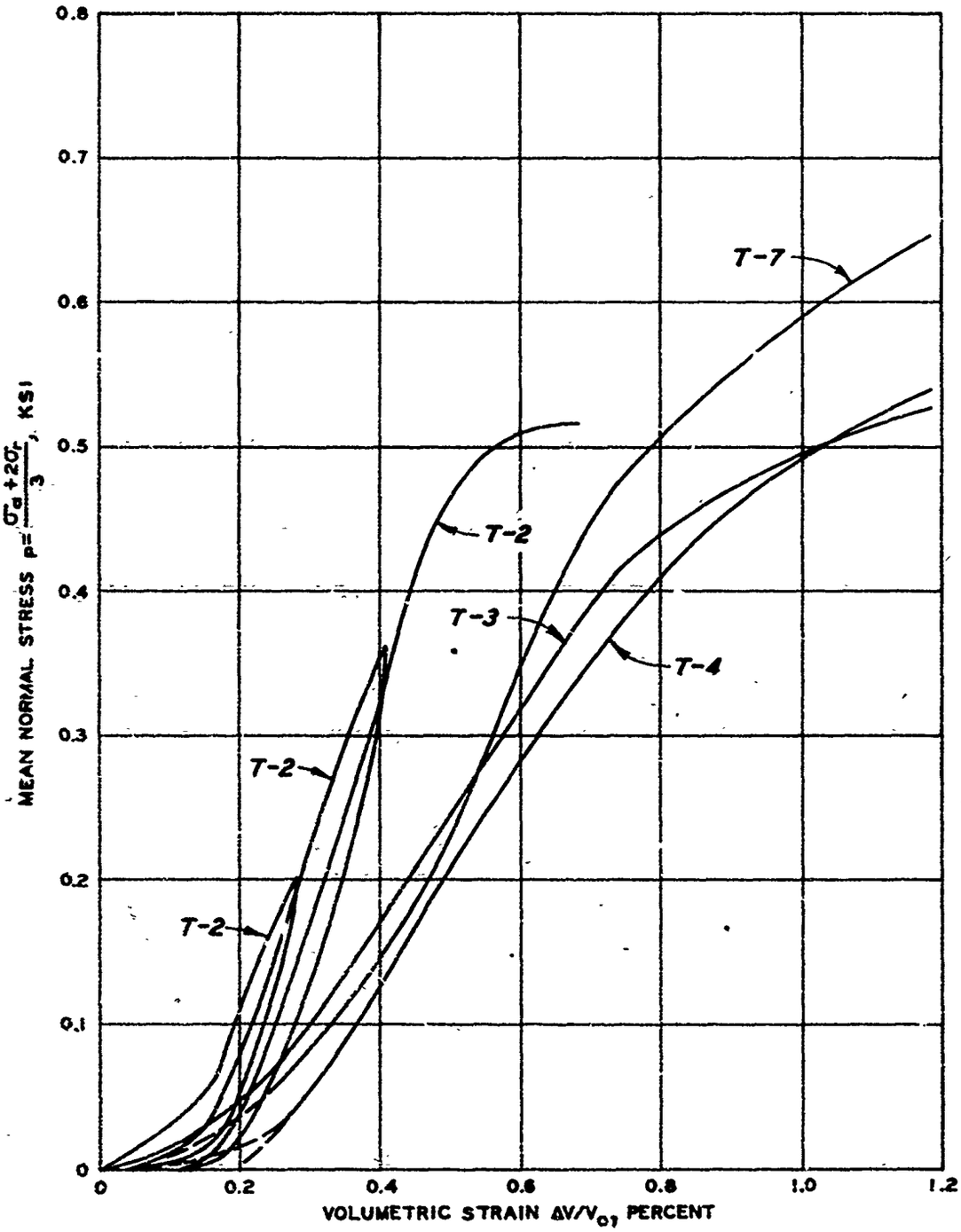

Figure 3.7 Initial loading portion of several static hydrostatic tests.

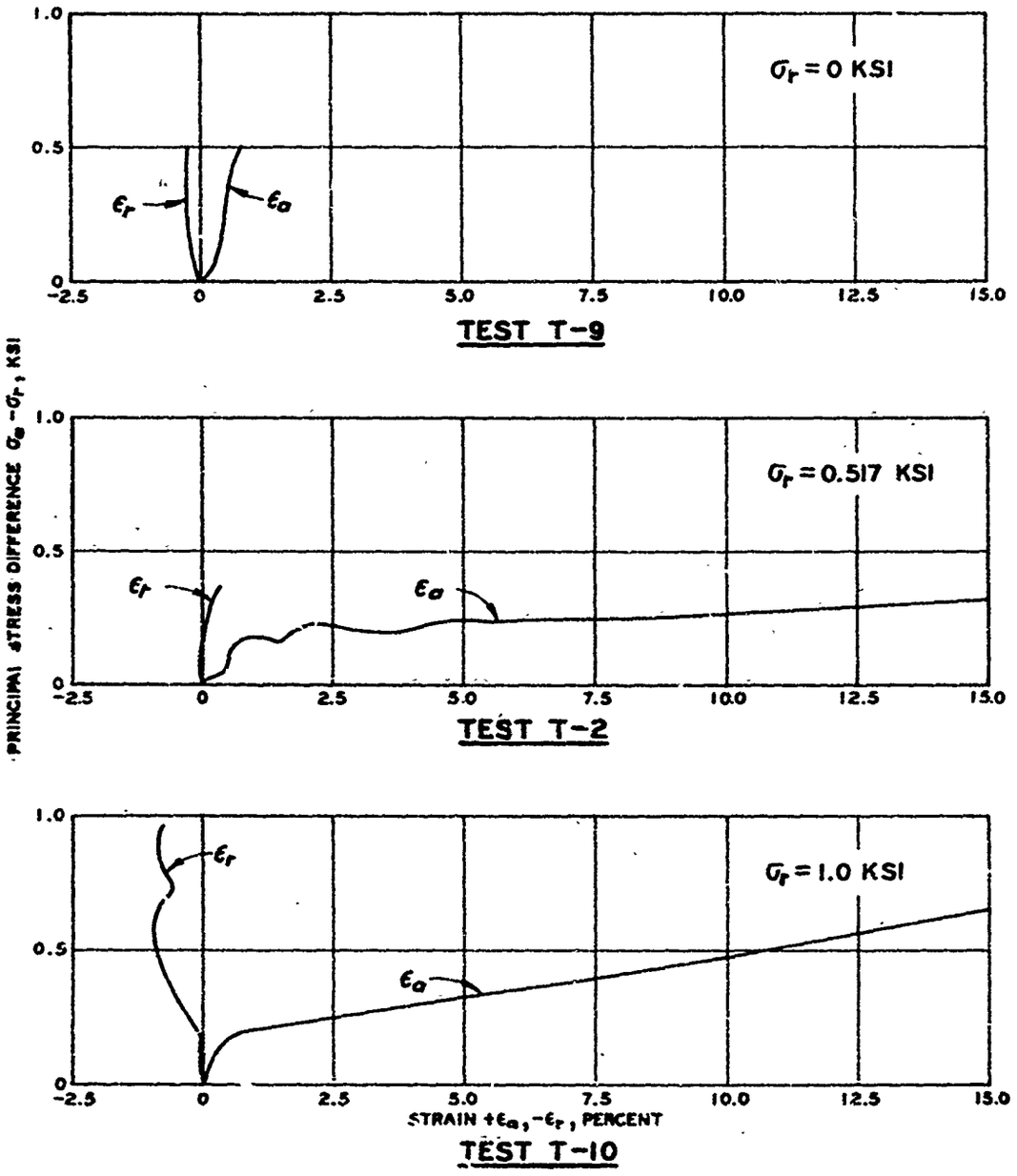

Figure 3.8 Static triaxial test results; Tests T-9, T-2, and T-10.

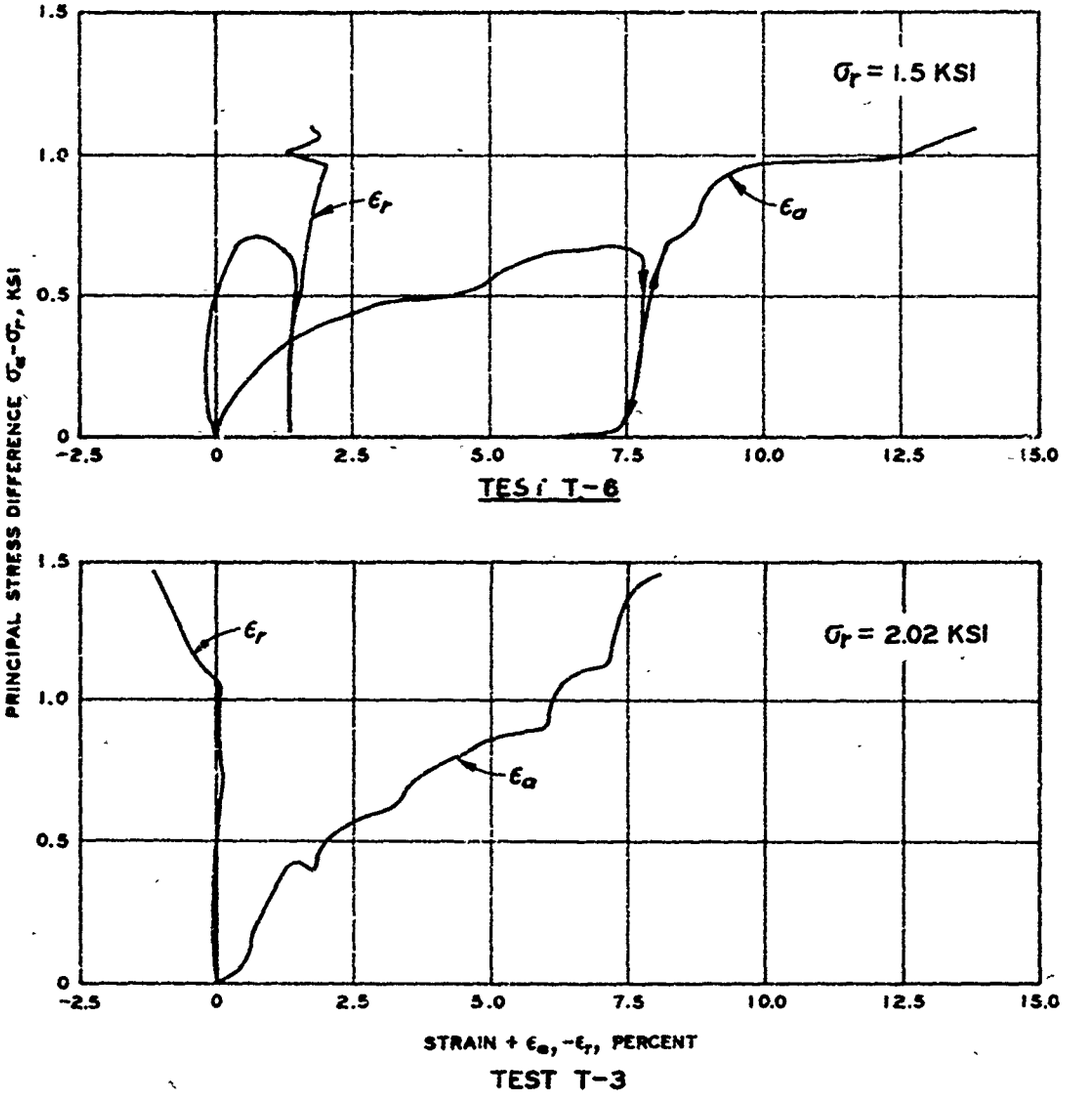

Figure 3.9 Static triaxial test results; Tests T-6 and T-3.

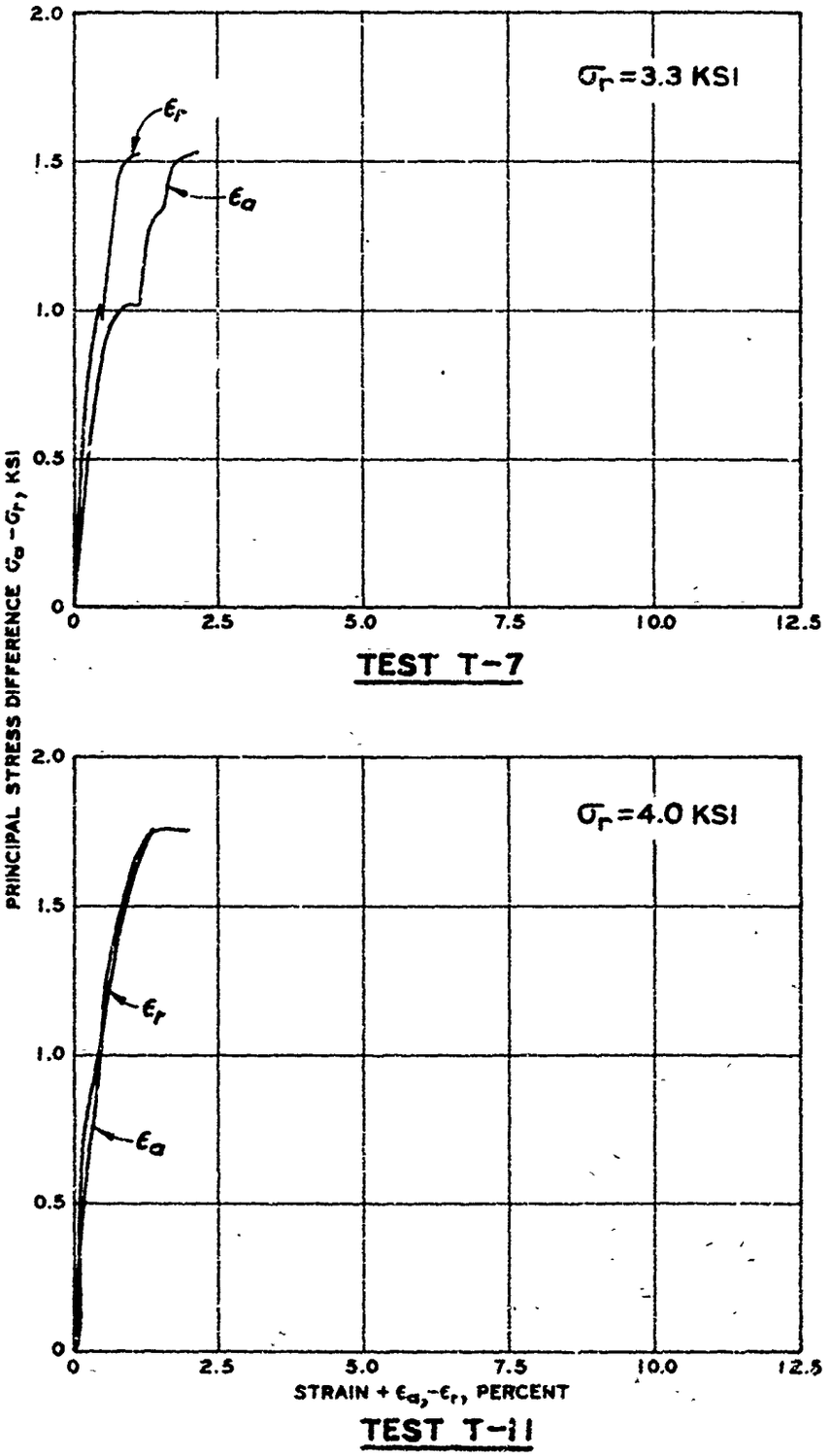

Figure 3.10 Static triaxial test results; Tests T-7 and T-11.

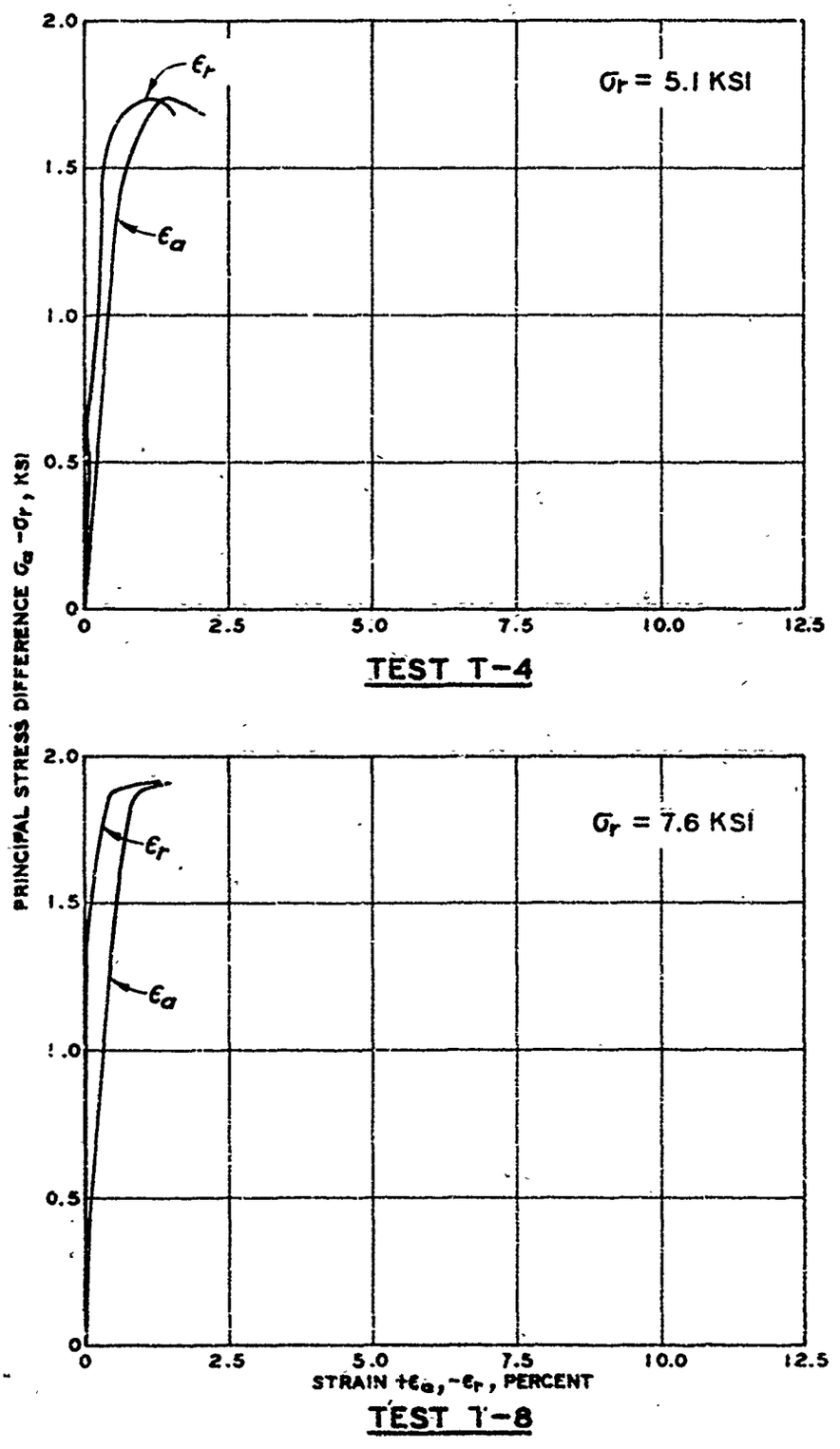

Figure 3.11 Static triaxial test results; Tests T-4 and T-8.

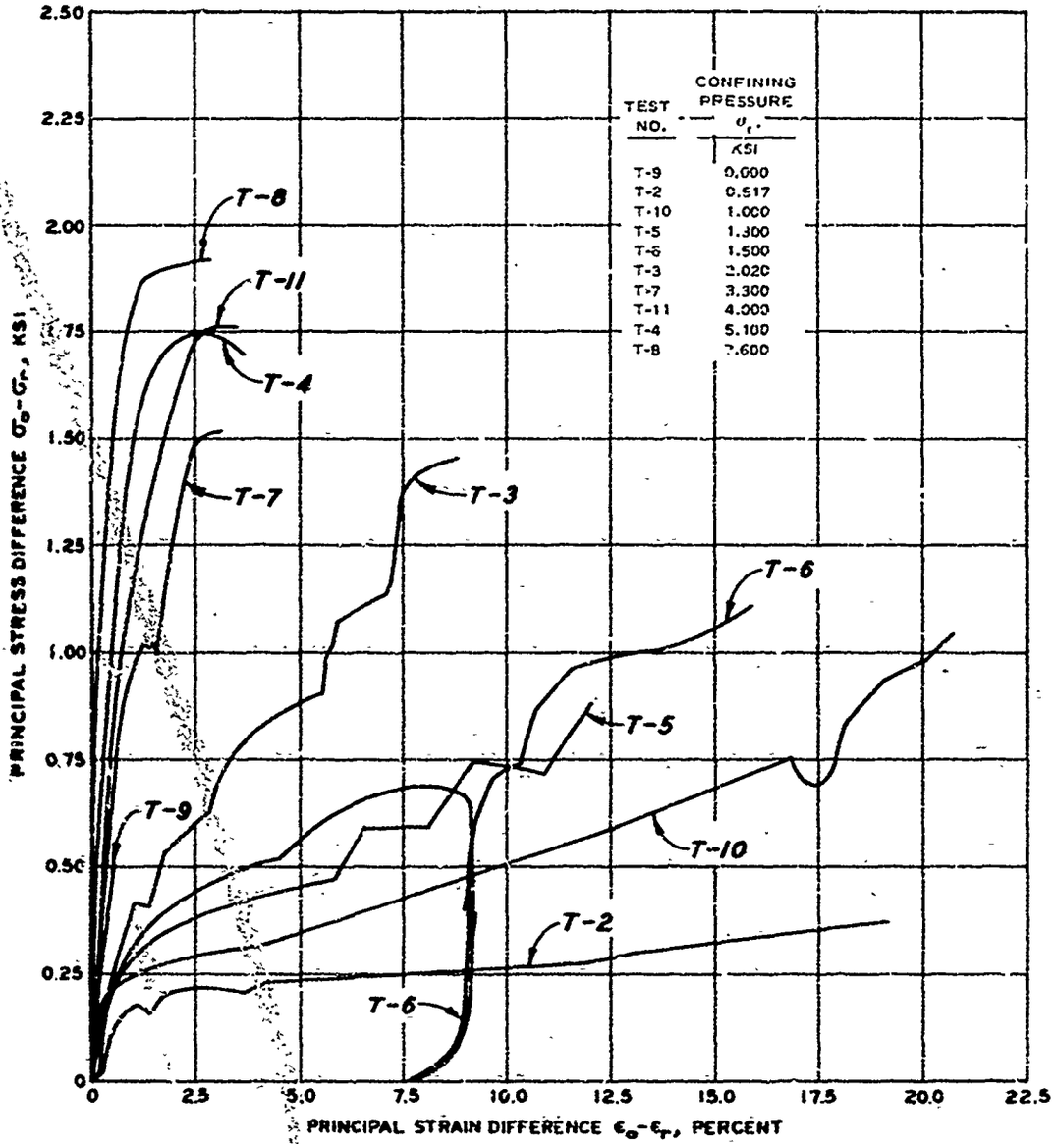

Figure 3.12 Combined plot of static triaxial test results.

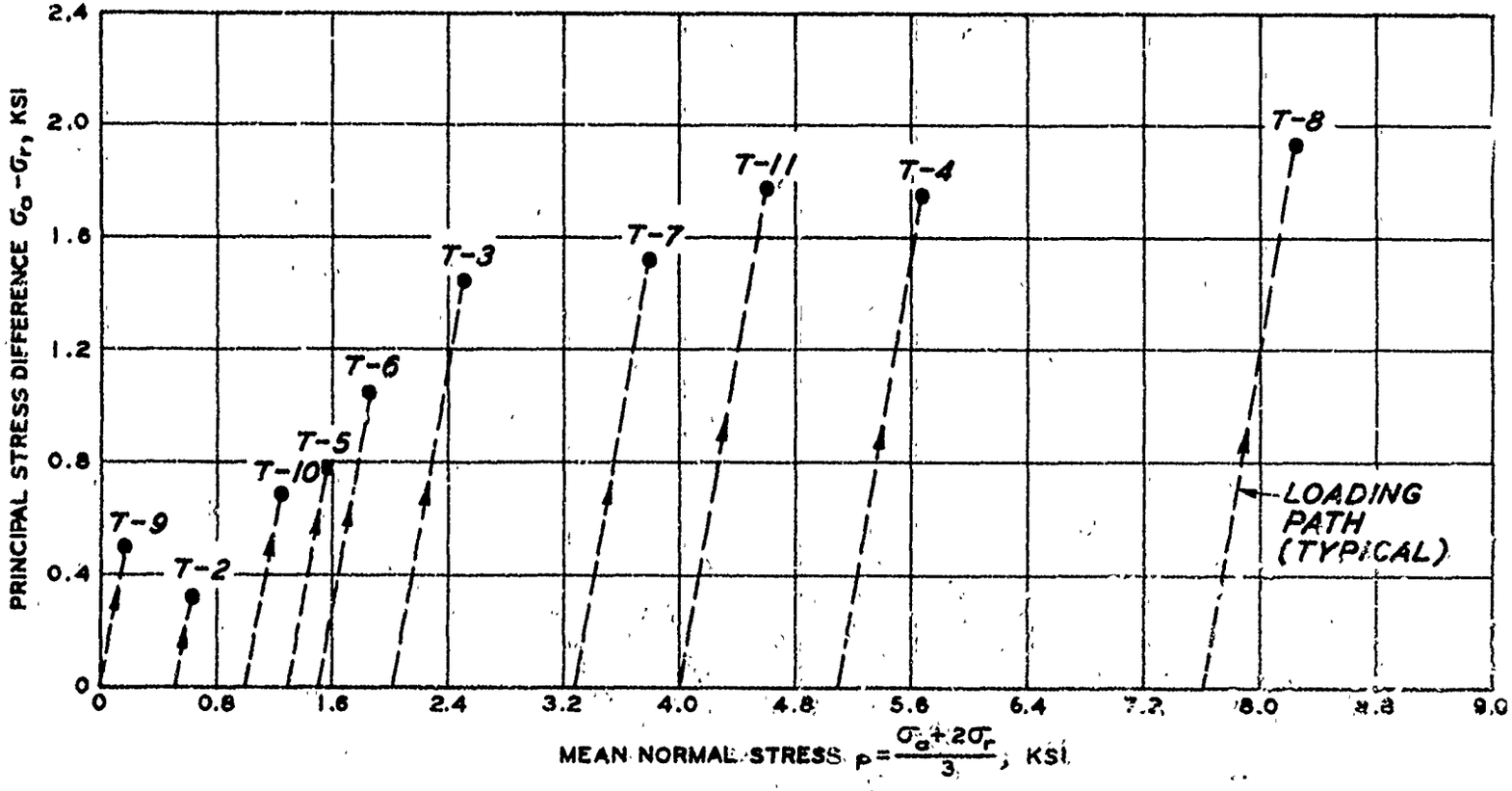

Figure 3.13 Static triaxial failure data.

CHAPTER 4

DISCUSSION OF TEST RESULTS

The test results presented in Chapter 3 represent the laboratory experimental investigation conducted for this study. The general data trend for each test condition and the suspect data were noted. In this chapter, the most representative material response for each particular imposed stress condition on a 62-pcf-density mix with a 60-day cure time will be presented and discussed. The selection of representative data is based on laboratory experience, knowledge of the particular test devices and measurement systems, and a general consideration of the response of the material in the other states of stress tested. The reader is cautioned that such representative data do not necessarily represent the best possible set of constitutive properties of cellular concrete, since exacting correlations between the several states of stress based on theoretical considerations were not performed.

4.1 UNIAXIAL RESPONSE

A series of eight UX tests and two null tests were conducted on cellular concrete with an imposed state of stress of no lateral strain. Of these tests, whose results are shown in Figures 3.1 and 3.2, only three, U-8, N-6, and N-9, were conducted on a concrete considered representative of a 62-pcf-density mix. The remaining tests were conducted on a drier concrete, probably with a greater air-void content. The test data above the 1,000-psi axial stress level in Test N-9 have previously been noted as being suspect, as were the very initial axial stress data (<20 psi) in Tests N-6, N-9, and U-8. It should also be noted that none of the tests were conducted at 60 day cure; however, beyond 40 days, cure time is believed to have only a small effect on the material properties. This belief is based on the results of the triaxial test series.

The most representative axial stress-strain response appears to be bounded by Tests U-8 and N-6, if the data from these tests are rezeroed to discount the initial strains at low (<25 psi) axial stress.

Figure 4.1 shows the estimated representative curve to 1 percent axial strain. It was not felt that the available test data were representative of the uniaxial strain response of a 62-pcf-density mix beyond 1 percent axial strain. However, the material should stiffen at smaller strain levels than those observed in Tests U-1 and U-4 because of the lower air-void content. The level of initial stiffening could be as low as 20 percent axial strain. Stiffening might continue to an axial stress level approaching 7,000 psi. At that level, the material should be nearly saturated, and the slope of the stress-strain curve might be at its maximum and be nearly equal to that of the hydrostatic, p versus $\Delta V/V_o$, plot. The secondary collapse phenomenon, noted previously in the hydrostatic tests, might also occur in UX tests at stress levels greater than 7,000-psi axial stress.

In the tests conducted, no significant differences were noted in the unloading-reloading response of the material. The axial deformation data obtained from Test N-6 were obtained with a lower-range measurement system that has greater resolution than the unloadings measured in the tests carried to large deformations. The material does not appear to be elastic even at low stress levels, and the unloading-reloading does not occur along the same stress-strain curve as the loading. Because at the high stress levels the resolution of the measurements was not as good as that in Test N-6, it was assumed for the purpose of this study that the unloading-reloading slopes do not change at higher stress levels. At very low stress levels (<20 psi) a rebounding occurs that can best be described as a hook in the stress-strain curve. The representative unloading curve is shown in Figure 4.1, and it is assumed that the slope given may be translated to higher stress levels.

4.2 UNIAXIAL STRESS PATH RESPONSE

The uniaxial stress path response of cellular concrete to high stress levels could not be obtained from the results of the null tests conducted because of limitations in the level of stress imposed by the null device. The data from the null tests must be considered in conjunction with the yield envelope from the TX test data. Since the yield

surface describes a lower limiting state of stress, the stress path from null tests on the material should lie within or on the yield surface. The null data can be used to describe the initial portion of the stress path, and the yield envelope can be used to describe the uniaxial stress path at higher stress levels; i.e., an assumption has been made that the material has yielded by the time high stress levels have been achieved. Therefore, it was assumed that the loading uniaxial stress path intercepts and follows the yield envelope described by the TX data above $p = 0.5$ ksi. It should be noted that this assumption could be in error, since the relations which exist between the uniaxial stress path and the yield surface of various materials are not completely understood, and the area is currently a source of continuing research. Additional null tests should be conducted to high stress levels, i.e., 5,000 psi, in an attempt to verify the assumption made here. Also, since no unloading data from stress levels above $p = 1$ ksi were available, the unloading response was assumed based on the available unloading bulk and shear moduli (stress path slope = $2G/K$).

Figure 4.2 shows a plot of the complete recommended uniaxial stress path. The initial loading portion to $p = 0.4$ ksi was based on the two null tests. The remainder of the loading path follows the TX yield envelope. The initial portion of the loading path is shown to an enlarged scale in Figure 4.3.

The unloading path, as previously mentioned, was based on the representative unloading bulk K and shear G moduli where the slope of the stress path S can be described as equal to $2G/K$. Because additional data were unavailable, it was assumed that the unloading slope could be translated to all levels of p.

The lower or negative uniaxial stress path was made symmetrical to the positive uniaxial stress path except at $p < 0.8$ ksi. The negative portion below $p = 0.8$ ksi was adjusted to reflect a loss of bond strength. It should be noted that the material, when loaded to high levels of p (i.e., $p > 1$ ksi) and then unloaded, did not crumble or fall apart when handled. This observation indicates the material was compacted and possessed some cohesive strength, the extent of which

should be evaluated by future study. The intercept was assumed to be at $p = -0.05$ ksi. One other important aspect of the negative path should be noted: If the material is loaded to a stress level below that associated with structural collapse and then unloaded, the bond strength is preserved; therefore, the negative path could be in error.

The slope of the uniaxial stress path is also related to Poisson's ratio for an incremental elastic medium in uniaxial strain as described in Section 3.2. Figure 4.4 shows a plot of loading Poisson's ratio ν versus mean normal stress as calculated from the representative uniaxial stress path previously shown in Figure 4.2 under the assumption of incremental elastic behavior. The initial Poisson's ratio ν of 0.25 appears reasonable, but the plot indicates a large variation in ν versus mean normal stress as the material is loaded to successively higher stress levels. It should be noted that the plot is only valid for one state of loading, uniaxial strain, and the values of ν may be different if determined for other states of stress which may exist, such as loading under conditions of a constant stress ratio.

4.3 HYDROSTATIC RESPONSE

The test results from the hydrostatic loading tests, shown in Figures 3.5 through 3.7, appear to be very consistent. The lower numbered tests, such as T-3 and T-4, were conducted at earlier cure times and began structural collapse at slightly lower stress levels, a development which is reasonable since the bond strength may not have developed fully during the shorter cure time. This effect was also noted in the UX test results. The specimen for Test T-4, as noted previously, appeared to contain a hard spot that is reflected by its higher density. The representative response selected was based on an average of Tests T-6 through T-11.

Figure 4.5 shows a plot of the representative hydrostatic response based on the actual test data. The initial slope, except for the initial 20 psi, was based on Test T-2 and is shown in the insert in Figure 4.5. At higher levels of stress, the curve is based on a weighted average of Tests T-6 through T-11. The unloading-reloading response has

the same characteristics as that noted for the uniaxial response, although the amount of the hook in the unloading-reloading might not be as great as that noted in Test T-4.

Tangent slopes of the representative hydrostat curve shown in Figure 4.5 may be used to construct a plot of bulk modulus K versus mean normal stress. Figure 4.6 shows such a plot and may be used to describe bulk modulus as a function of mean normal stress. The initial value of $K = 125$ ksi appears reasonable, followed by a rapid decrease and then a gradual increase to a maximum value of 400 ksi at $p > 4.5$ ksi.

4.4 SHEAR RESPONSE

The results of the TX tests are presented as a plot of principal stress difference versus principal strain difference in Figure 3.12. These results were smoothed to construct representative principal stress difference/principal strain difference plots shown in Figure 4.7. The slope of each plot is two times the shear modulus G. The initial loading values of G were selected from each of the curves and are presented in Figure 4.8 as a plot of initial loading shear modulus G_i versus mean normal stress. The plot indicates that G_i is a function of p and that G_i increases as p increases. Test T-9 has a higher value of G_i than that indicated by the G_i data from tests at $p < 2$ ksi. It is not known if Test T-9 is in error or if the response is reasonable. The other shear tests, T-2, T-10, etc., were conducted after some level of p had been applied to the material; therefore, initiation of microfracturing of the bonds in the material might result in a lower G_i at intermediate confining pressure levels ($p < 0.5$ ksi).

Figure 4.8 does not, however, represent the complete shear response of cellular concrete, since it can be seen from Figure 4.7 that the slope of the stress-strain curve is also changing as principal stress difference changes. For each test, the tangent shear modulus was determined at various stress difference levels. Figure 4.9 shows the results as a plot of principal stress difference versus shear modulus. Each curve represents one shear test at a given confining pressure,

i.e., p not constant. The curves show the general variation of G with principal stress difference: G decreases as $\sigma_a - \sigma_r$ increases. In general, the plot indicates that under the assumption of an incrementally elastic material, the loading shear modulus for cellular concrete may be described as a function of both mean normal stress and principal stress difference.

To illustrate how G varies, a three-dimensional sketch is shown in Figure 4.10. The Y-X axis of principal stress difference versus mean normal stress, respectively, contains the representative failure envelope and the loading path of each shear test (shown as a dashed line). The X-Z axis of mean normal stress versus shear modulus contains the initial shear modulus data (connected by a dashed line) previously shown in Figure 4.8. The family of curves shown previously in Figure 4.9 is contained in the three-dimensional space. Whether the surface describing G , which has been generated by the TX test data, is applicable to other loading states of stress, such as a constant p loading, is not known.

4.5 SUMMARY OF REPRESENTATIVE DATA

The previous sections include the recommended representative static stress-strain response of cellular concrete under various states of stress. The sections also include the static moduli values and their variations with one or more conditions of loading. Such information, however, does not constitute the complete understanding of the material. For example, it can be shown that the representative hydrostatic stress-strain curve may not be applicable to infer the volumetric strain response of the material loaded to a given level of p and then loaded to some level of principal stress difference. Figure 4.11 shows a plot of the representative hydrostatic response. Superimposed on that plot are the volumetric strain data measured during each of the shear tests. The data reflect the actual level of mean normal stress to which the material was subjected. The results indicate increased compaction with increasing principal stress difference at levels of $p < 2.5$ ksi. At $p > 3$ ksi, the material dilates or shows expansion at

increasing levels of principal stress difference. Therefore, there may only be one unique level of mean normal stress where the volumetric strain response is independent of level of principal stress difference for this particular density. The interrelation of the response of the material under various states of stress as observed from the laboratory test data must be considered in the development of constitutive relations.

One other point should be discussed. Almost all of the tests that were performed and all of the representative curves that were developed are for a static undrained loading condition. The limited dynamic UX test results shown previously in Figure 3.3, when compared with static tests on similarly cured material, indicate a rate effect. This rate effect may be applicable to most loading conditions. It is believed that the form of the dynamic stress-strain relations for this material may be similar to the static relations.

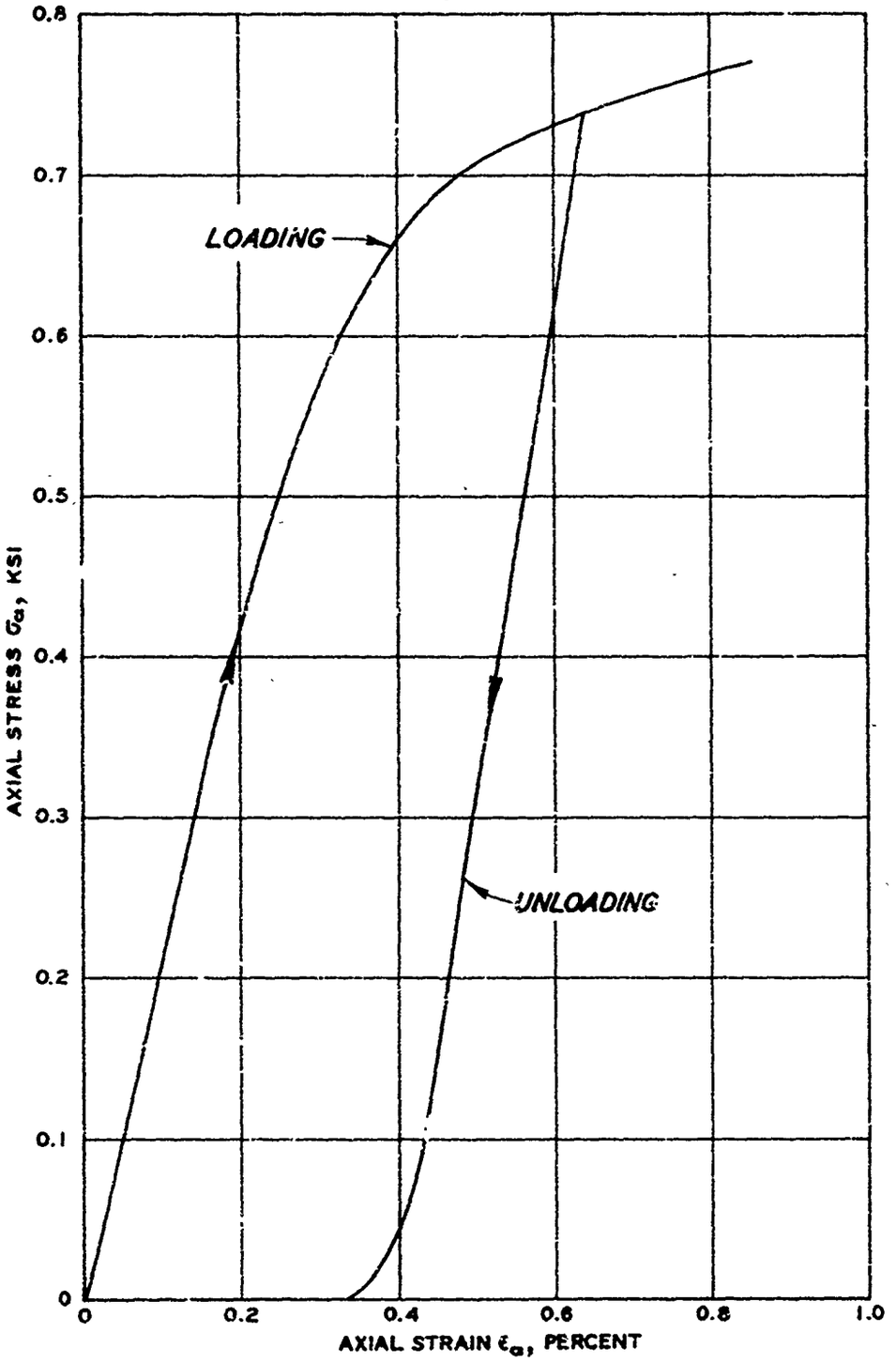

Figure 4.1 Representative static uniaxial response.

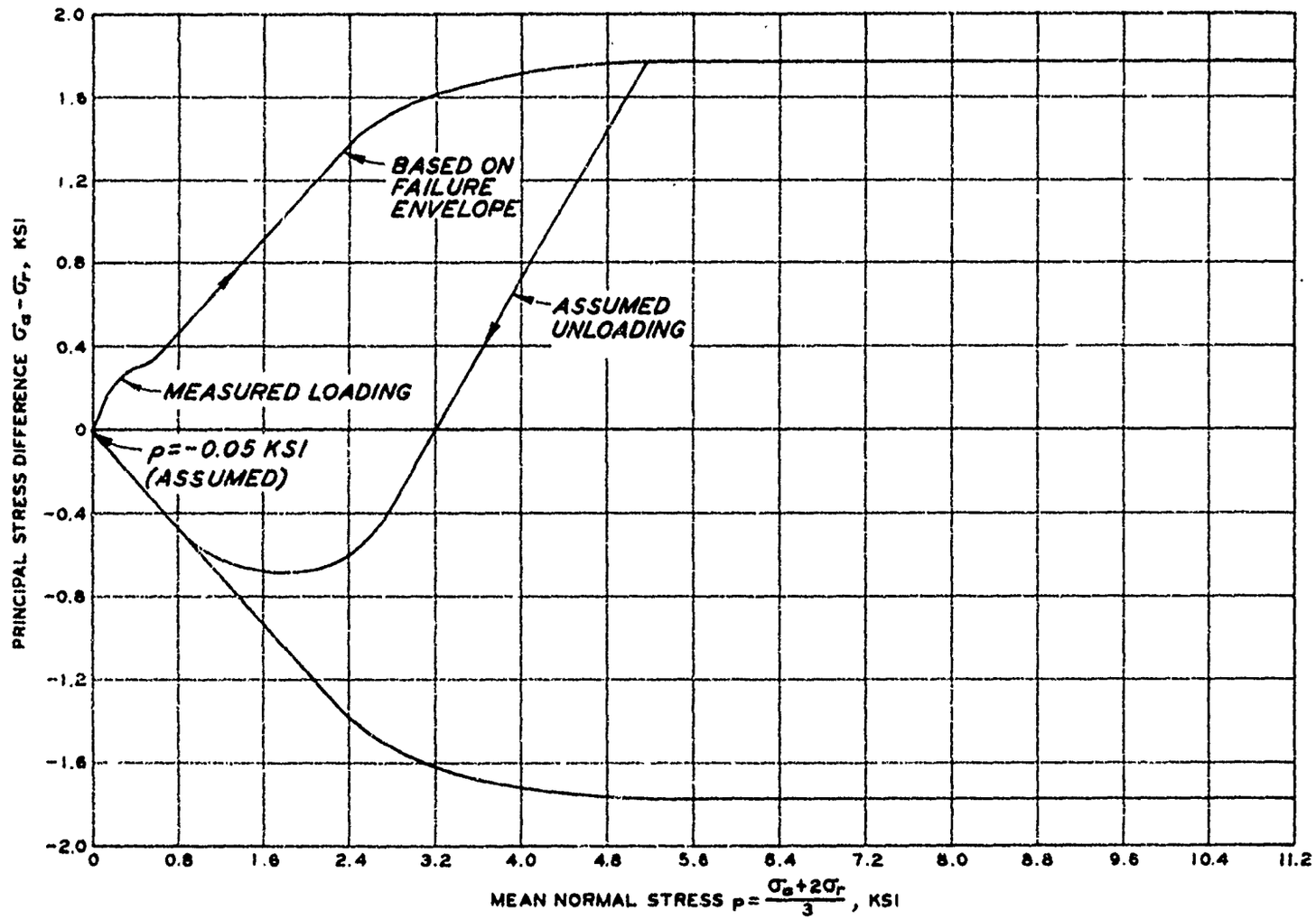

Figure 4.2 Assumed static uniaxial stress path for cellular concrete.

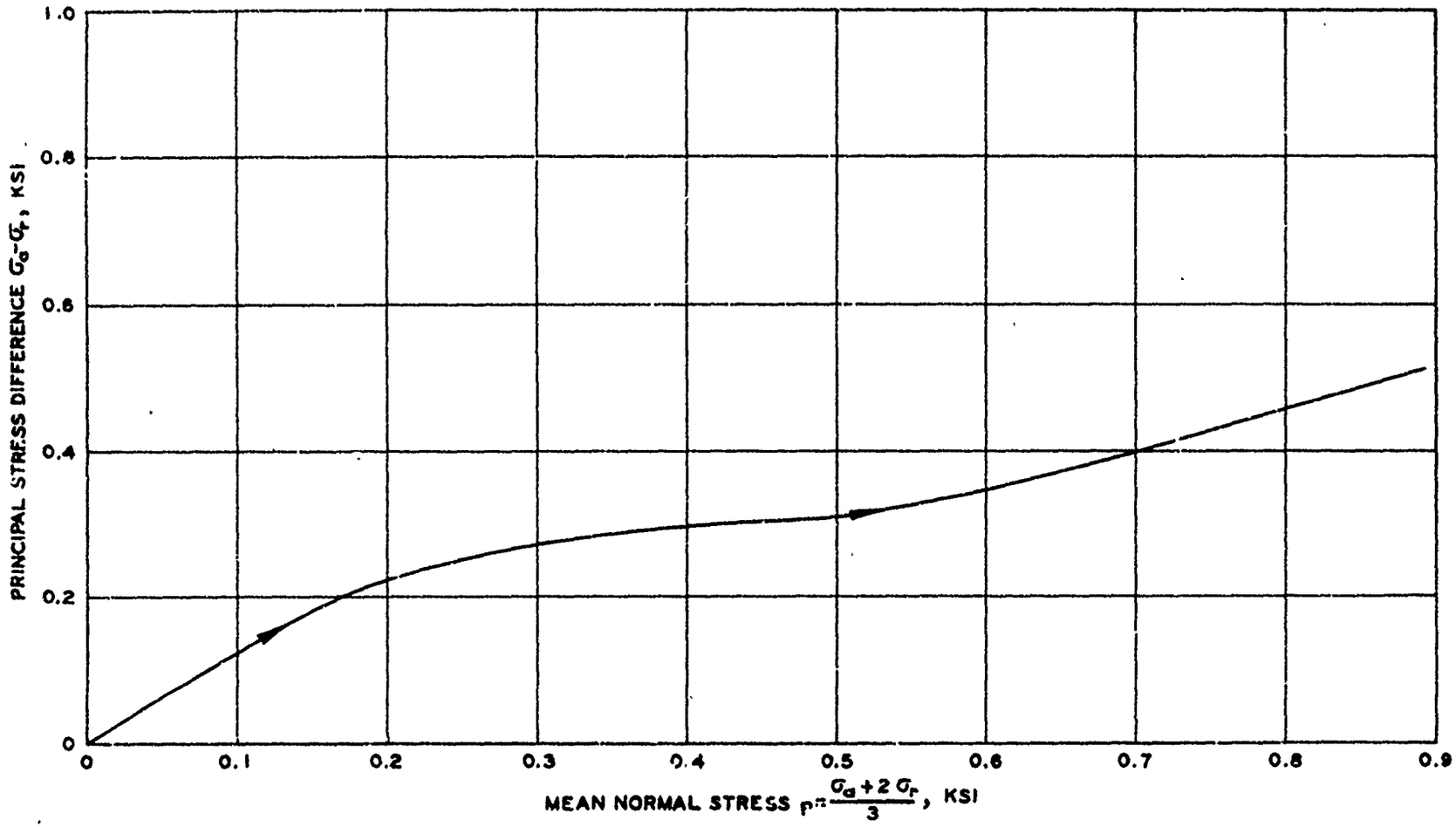

Figure 4.3 Initial loading path of representative static uniaxial stress path.

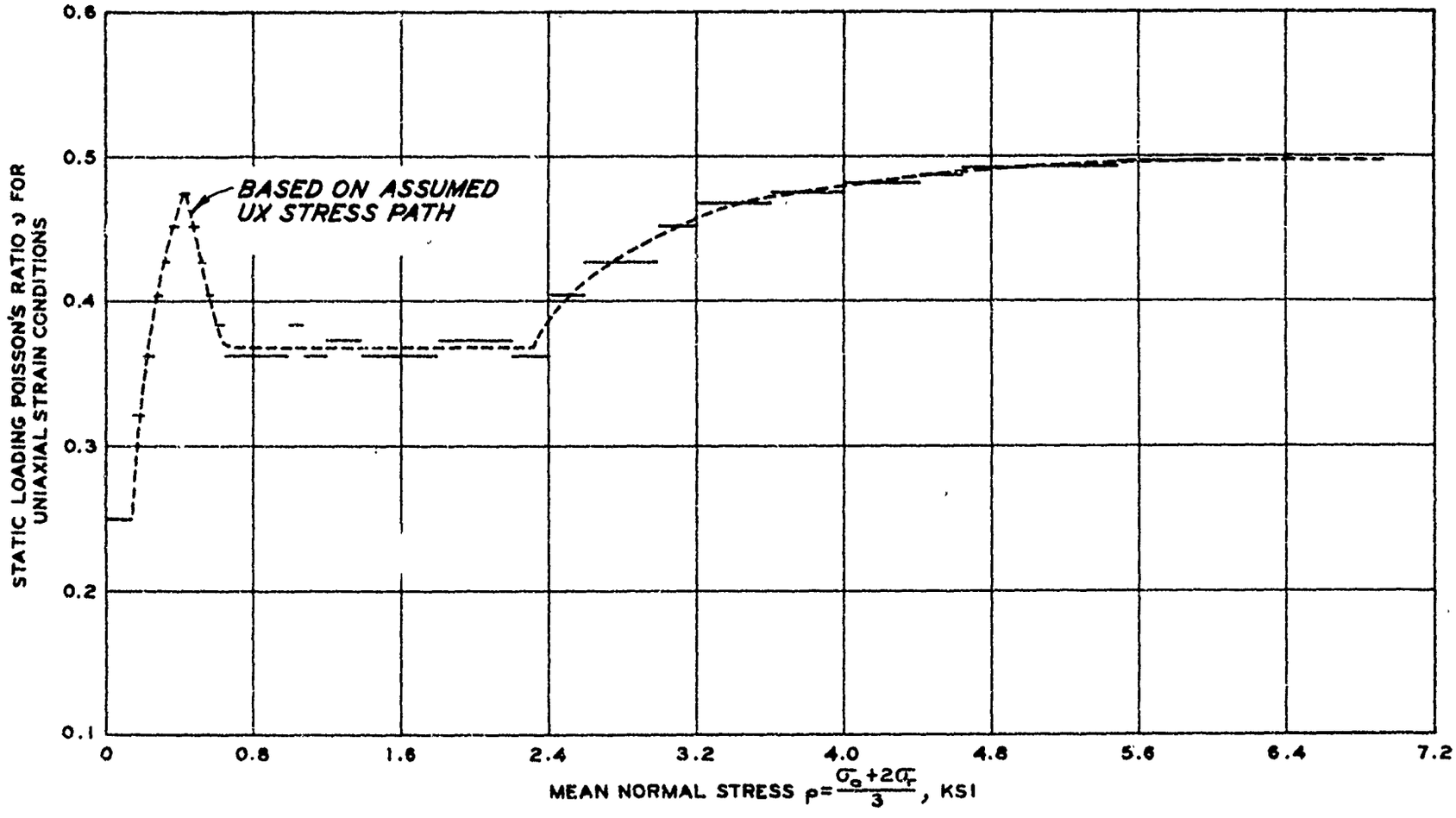

Figure 4.4 Plot of Poisson's ratio versus mean normal stress for conditions of uniaxial strain.

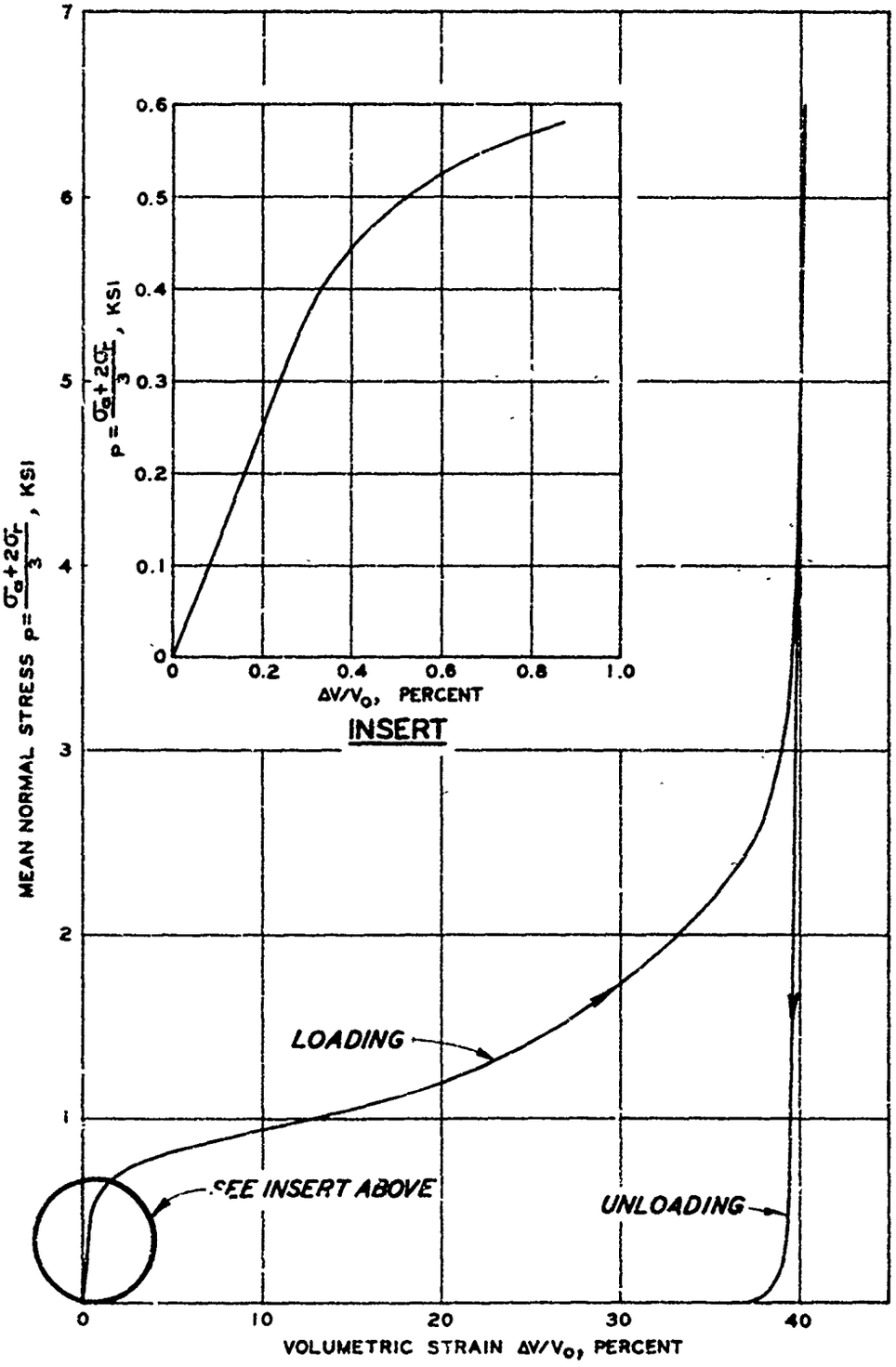

Figure 4.5 Representative static hydrostatic response.

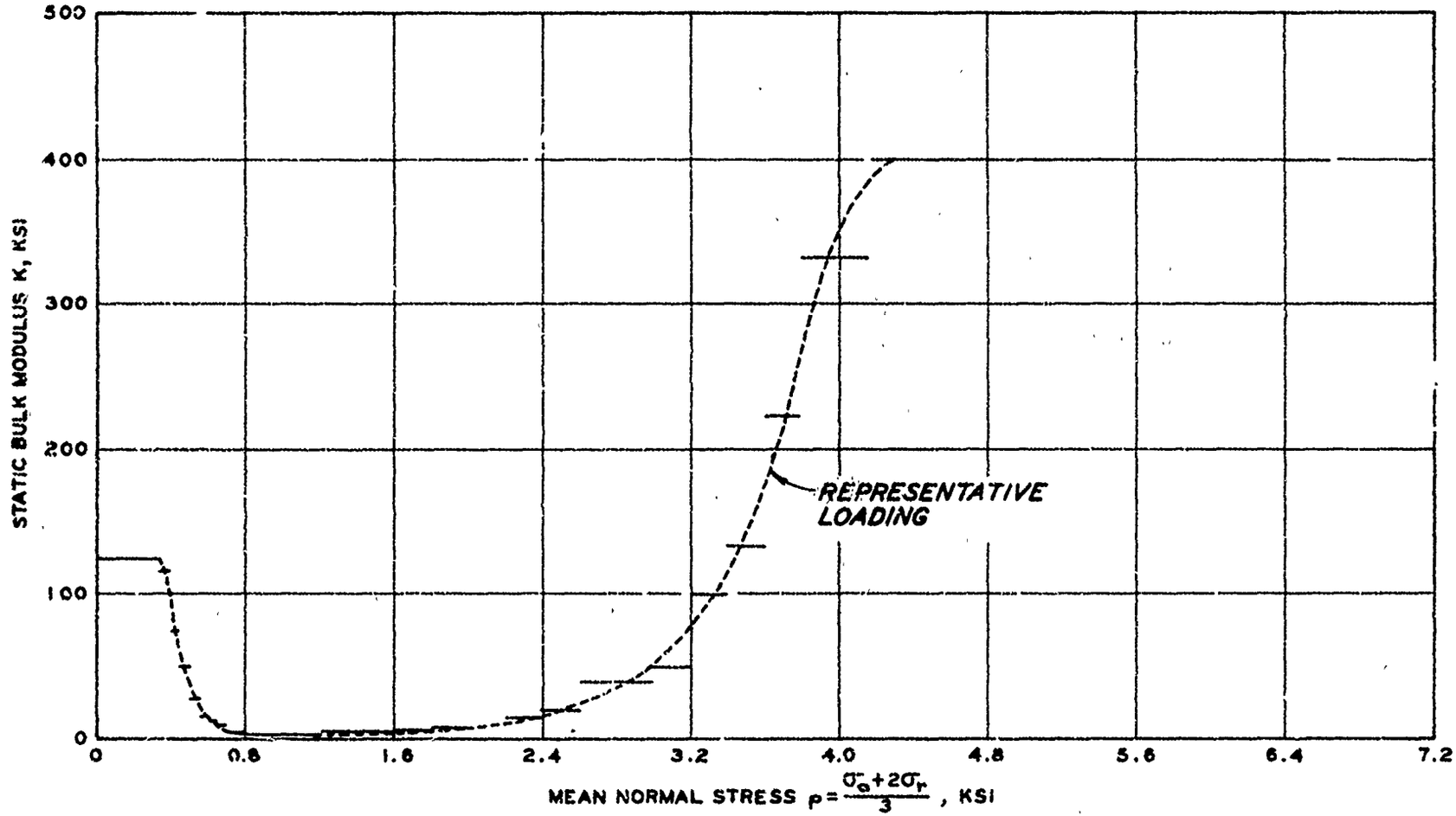

Figure 4.6 Plot of bulk modulus versus mean normal stress.

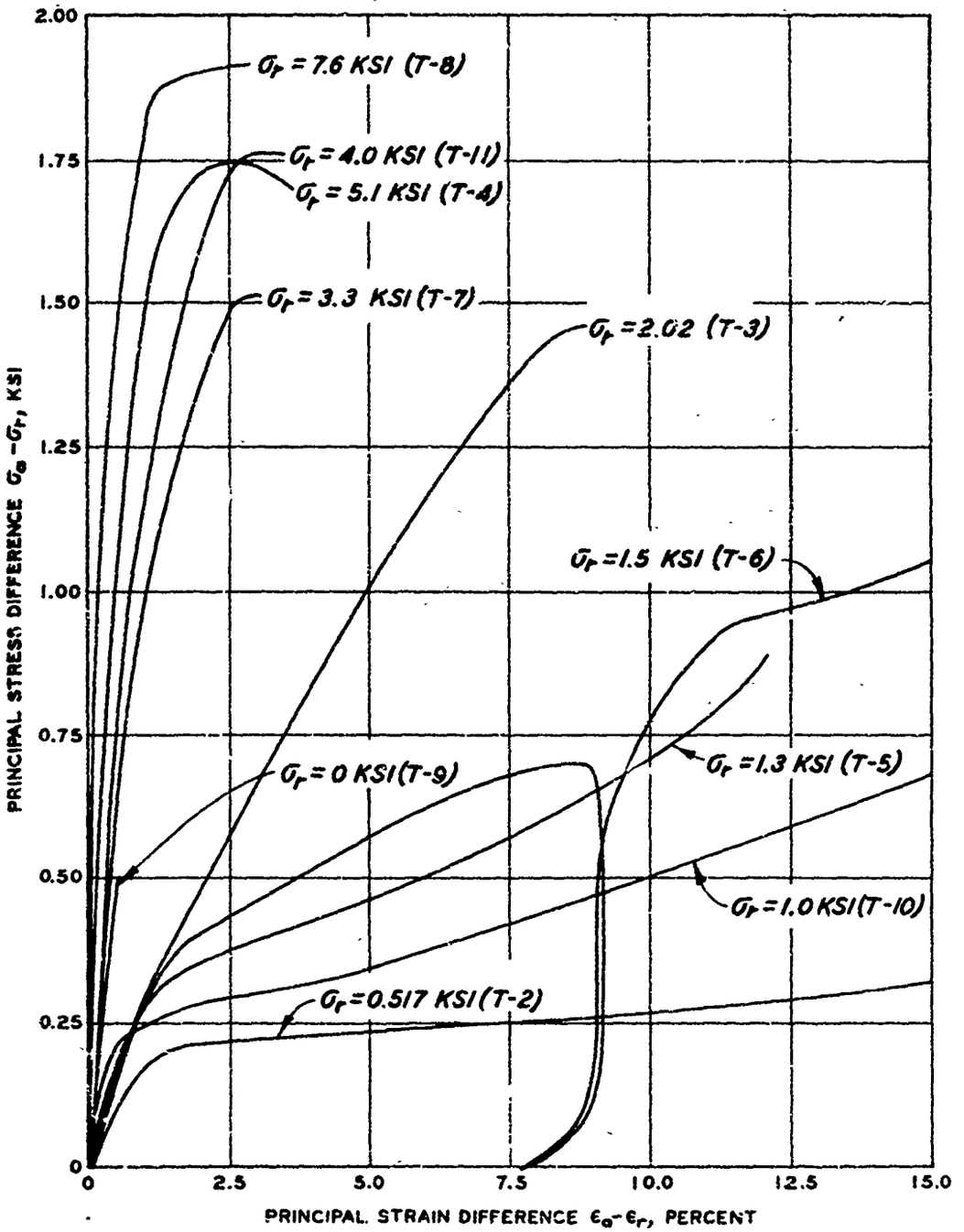

Figure 4.7 Representative static triaxial shear response for various confining pressures.

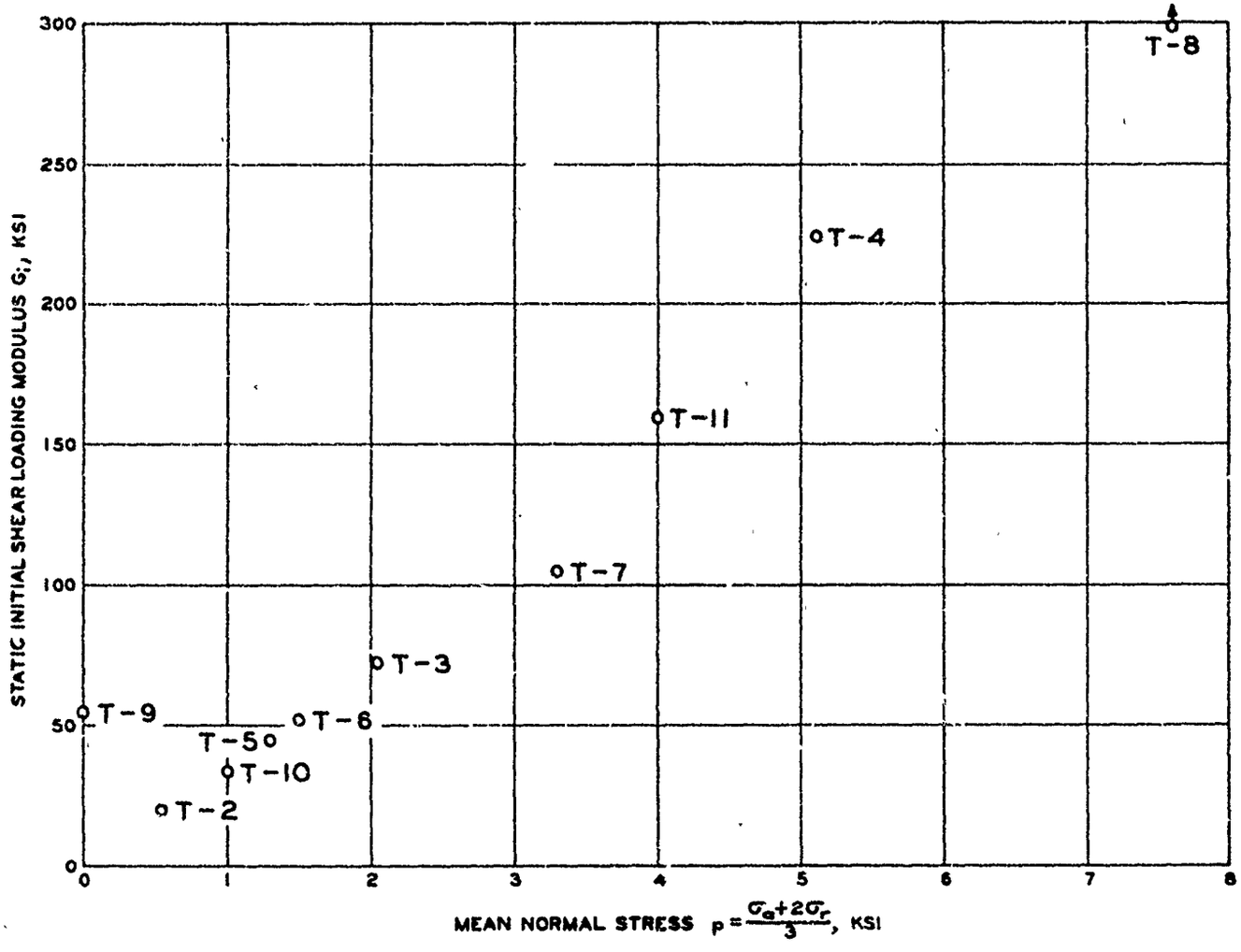

Figure 4.8 Plot of initial loading shear modulus versus mean normal stress based on triaxial tests.

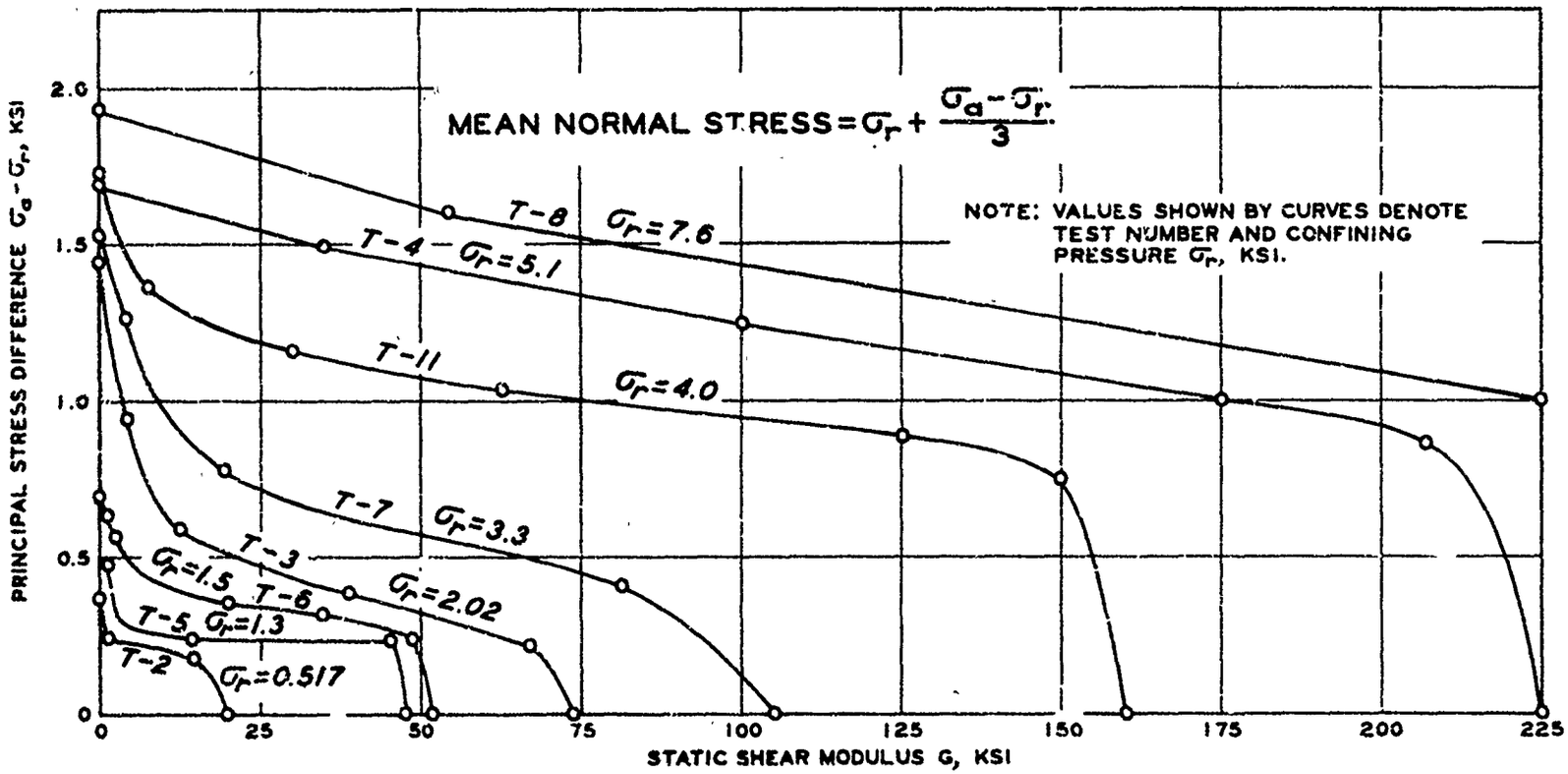

Figure 4.9 Plot of principal stress difference versus shear modulus based on triaxial tests.

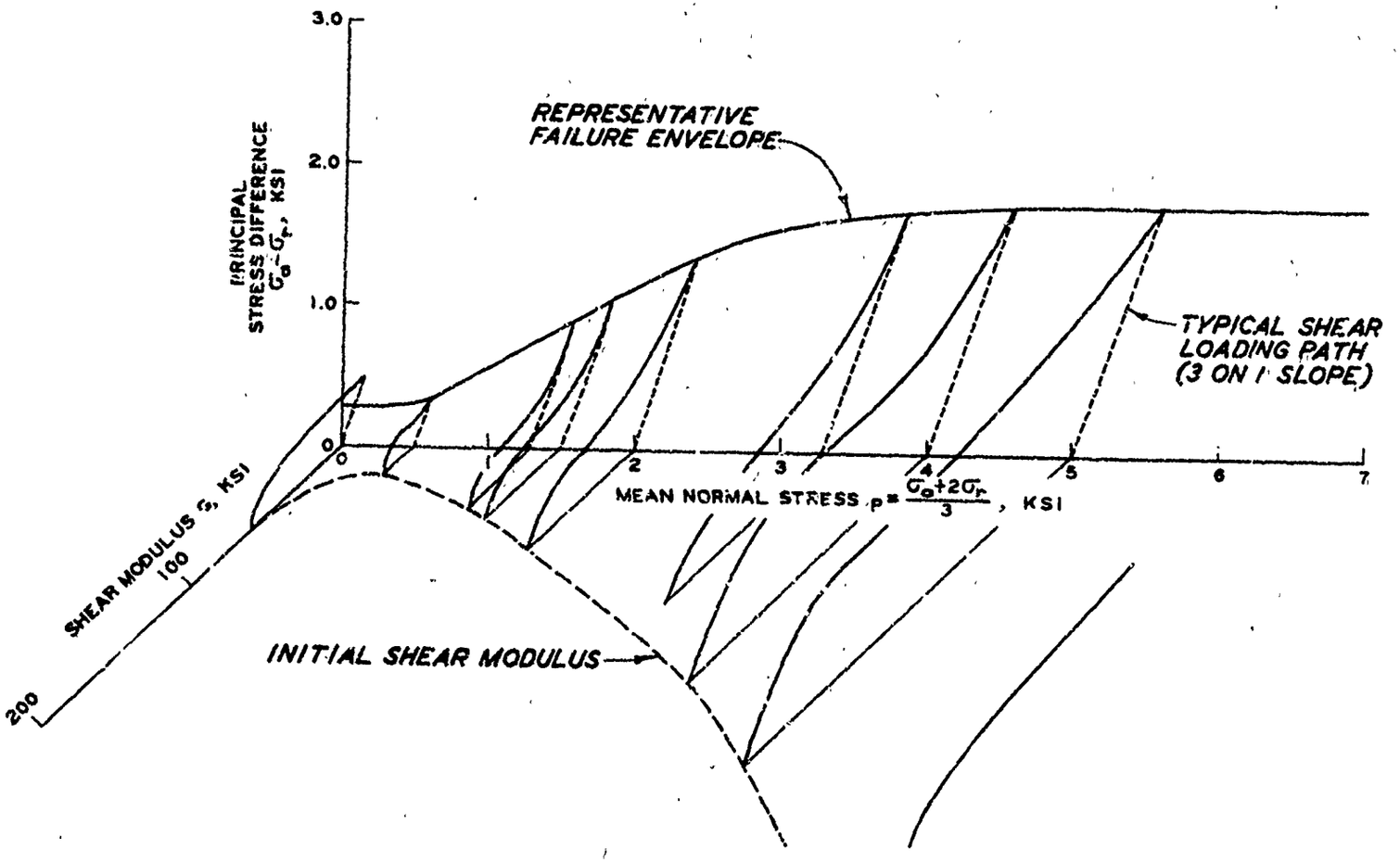

Figure 4.10 Sketch indicating variation of shear modulus with principal stress difference and mean normal stress.

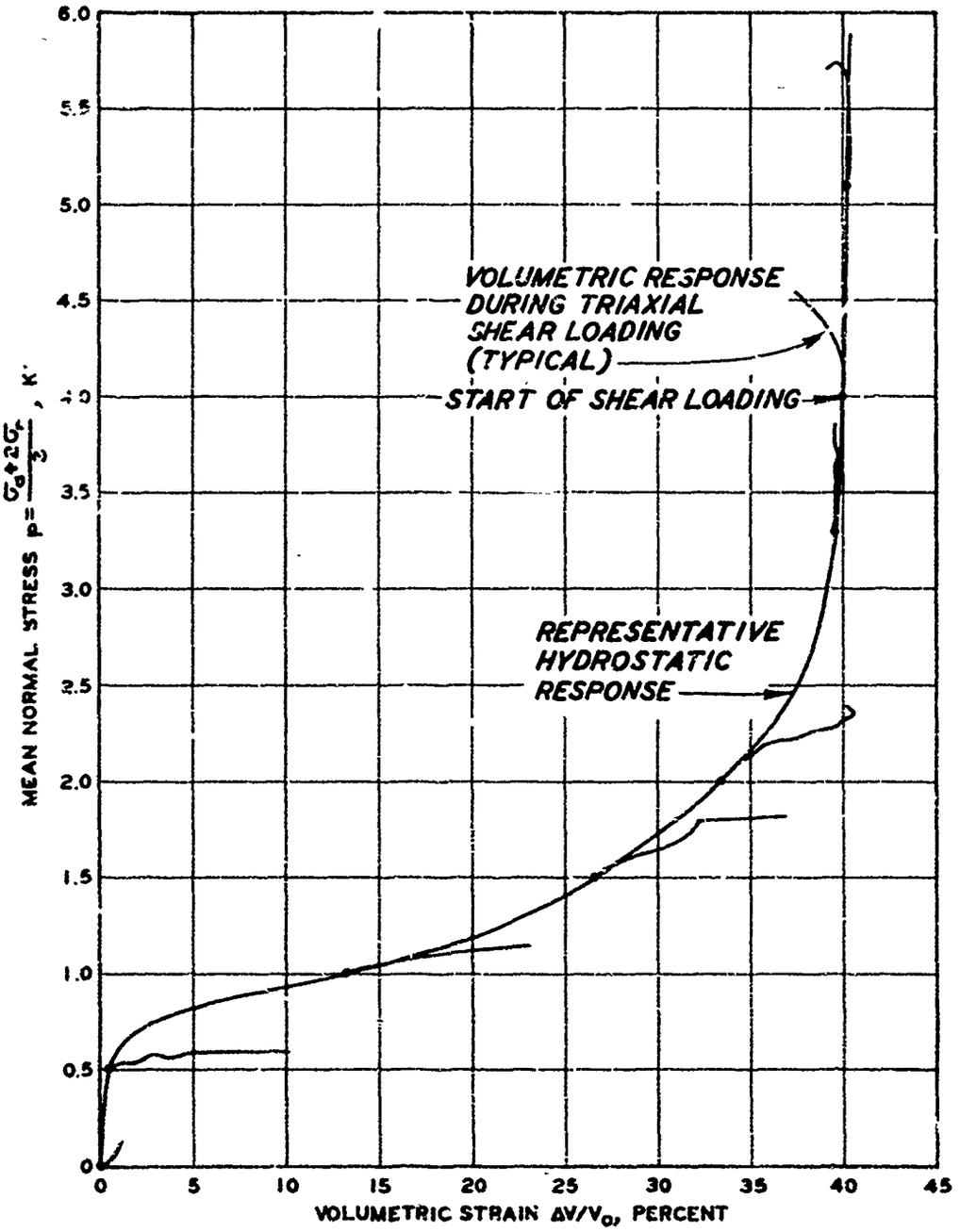

Figure 4.11 Plot of volumetric strain response during triaxial shear superimposed on representative hydrostatic loading curve.

CHAPTER 5

SUMMARY AND RECOMMENDATIONS

5.1 SUMMARY

The purpose of this study was to determine the representative stress-strain properties of cellular concrete under various states of stress that would be needed for the derivation of constitutive relations.

A series of static UX tests, null tests, and hydrostatic and TX shear tests were conducted. The results of these tests were presented as a series of stress-strain curves and stress path plots. From these data and certain assumptions, representative stress-strain relations were selected to represent the static response of a 60-day-cure, 62-pcf-density mix of cellular concrete.

Assumptions were required in the derivation of the representative data where the actual data were questionable or lacking. Included in those assumptions were the following: (1) The uniaxial stress path at mean normal stress levels above 0.6 ksi was assumed to follow the failure envelope. (2) The unloading uniaxial stress path was assumed to be independent of principal stress difference. (3) The lower yield envelope was assumed to be nearly symmetrical with the upper envelope. (4) A tension cutoff of -0.05 ksi was assumed.

The dynamic response of cellular concrete was not investigated in this study; however, three dynamic UX tests were conducted. The results indicate that the response of the material is affected by the rate of loading.

5.2 RECOMMENDATIONS

The following additional tests are recommended to supplement the existing data:

1. Static UX tests should be conducted to 3 ksi with unloading at several stress levels. Null or K_o tests, with unloading, to a level of p associated with lockup should also be conducted. The purpose of these tests will be to fill the previously mentioned gaps in

available data and to verify various assumptions that were made in this report.

2. A limited series of dynamic UX and TX tests should be conducted at a stress rate similar to that expected in the field loading. Consideration should be given to the uniaxial stress-strain response and shear strength. The purpose of such a test series will be to allow adjustment of static data to reflect stress rate effects, since the limited dynamic UX data indicate loading rate effects on both the initial modulus and the level of structural breakdown of the material.

REFERENCES

1. G. C. Hoff; "Shock-Absorbing Materials, Cellular Concrete as a Backpacking Material"; Technical Report No. 6-763. Report 2, June 1971; U. S. Army Engineer Waterways Experiment Station, CE; Vicksburg, Mississippi; Unclassified.

2. L. Schindler; "Design and Evaluation of a Device for Determining the One-Dimensional Compression Characteristics of Soils Subjected to Impulsive-Type Loads"; Technical Report S-68-9, November 1968; U. S. Army Engineer Waterways Experiment Station, CE; Vicksburg, Mississippi; Unclassified.